Title
Airborne tunable diode laser measurements of formaldehyde during TRACE-P: Distributions and box model comparisons

Journal
Journal of Geophysical Research, 108(D20)

ISSN
0148-0227

Authors
Fried, Alan
Crawford, James
Olson, Jennifer
et al.

Publication Date
2003

DOI
10.1029/2003jd003451

Airborne tunable diode laser measurements of formaldehyde during TRACE-P: Distributions and box model comparisons

Alan Fried,[1] James Crawford,[2] Jennifer Olson,[2] Jim Walega,[1] William Potter,[3] Bryan Wert,[1,4] Carolyn Jordan,[2] Bruce Anderson,[2] Rick Shetter,[1] Barry Lefer,[1] Donald Blake,[5] Nicola Blake,[5] Simone Meinardi,[5] Brian Heikes,[6] Daniel O'Sullivan,[7] Julie Snow,[6] Henry Fuelberg,[8] Christopher M. Kiley,[8] Scott Sandholm,[9] David Tan,[9] Glen Sachse,[2] Hanwant Singh,[10] Ian Faloona,[1] Charles N. Harward,[11] and Gregory R. Carmichael[12]

Received 24 January 2003; revised 8 May 2003; accepted 15 May 2003; published 23 September 2003.

[1] Airborne measurements of CH_2O were acquired employing tunable diode laser absorption spectroscopy during the 2001 Transport and Chemical Evolution Over the Pacific (TRACE-P) study onboard NASA's DC-8 aircraft. Above ~2.5 km, away from the most extreme pollution influences and heavy aerosol loadings, comprehensive comparisons with a steady state box model revealed agreement to within ±37 pptv in the measurement and model medians binned according to altitude and longitude. Likewise, a near unity slope (0.98 ± 0.03) was obtained from a bivariate fit of the measurements, averaged into 25 pptv model bins, versus the modeled concentrations for values up to ~450 pptv. Both observations suggest that there are no systematic biases on average between CH_2O measurements and box model results out to model values ~450 pptv. However, the model results progressively underpredict the observations at higher concentrations, possibly due to transport effects unaccounted for in the steady state model approach. The assumption of steady state also appears to contribute to the scatter observed in the point-by-point comparisons. The measurement-model variance was further studied employing horizontal flight legs. For background legs screened using a variety of nonmethane hydrocarbon (NMHC) tracers, measurement and model variance agreed to within 15%. By contrast, measurement variance was ~60% to 80% higher than the model variance, even with small to modest elevations in the NMHC tracers. Measurement-model comparisons of CH_2O in clouds and in the lower marine troposphere in the presence of marine aerosols suggest rather significant CH_2O uptake by as much as 85% in one extreme case compared to expectations based on modeled gas phase processes. *INDEX TERMS:* 0394 Atmospheric Composition and Structure: Instruments and techniques; 0368 Atmospheric Composition and Structure: Troposphere—constituent transport and chemistry; *KEYWORDS:* tunable diode laser, TRACE-P formaldehyde, airborne formaldehyde measurements

Citation: Fried, A., et al., Airborne tunable diode laser measurements of formaldehyde during TRACE-P: Distributions and box model comparisons, *J. Geophys. Res.*, *108*(D20), 8798, doi:10.1029/2003JD003451, 2003.

1. Introduction

[2] The chemistry and distribution of the reactive intermediate formaldehyde (CH_2O) has been of interest to atmospheric scientists for more than two decades. This gas, which is one of the most abundant gas phase carbonyl compounds found in the atmosphere, is formed by the oxidation of most anthropogenic and biogenic hydrocarbons initiated by reactions with the hydroxyl (OH) radical and

[1]Atmospheric Technology and Atmospheric Chemistry Divisions, National Center for Atmospheric Research, Boulder, Colorado, USA.
[2]Atmospheric Sciences Division, Langley Research Center, NASA, Hampton, Virginia, USA.
[3]Department of Chemistry and Biochemistry, University of Tulsa, Tulsa, Oklahoma, USA.
[4]Also at Department of Chemistry, University of Colorado, Boulder, Colorado, USA.
[5]Department of Chemistry, University of California, Irvine, California, USA.
[6]Graduate School of Oceanography/Center for Atmospheric Chemistry, University of Rhode Island, Narragansett, Rhode Island, USA.
[7]Department of Chemistry, U.S. Naval Academy, Annapolis, Maryland, USA.
[8]Department of Meteorology, Florida State University, Tallahassee, Florida, USA.
[9]School of Earth and Atmospheric Sciences, Georgia Institute of Technology, Atlanta, Georgia, USA.
[10]NASA Ames Research Center, Moffett Field, California, USA.
[11]Science Applications International Corporation, Langley Research Center, NASA, Hampton, Virginia, USA.
[12]Department of Chemical and Biochemical Engineering, University of Iowa, Iowa City, Iowa, USA.

0148-0227/03/2003JD003451

ozone (O_3). Over continental areas, oxidation of nonmethane hydrocarbons (NMHCs) dominates the production of CH_2O [*Fried et al.*, 1997b]. This gas is emitted directly by incomplete fossil fuel combustion as well as from secondary processes [*de Serves*, 1994; *Sigsby et al.*, 1987]. Formaldehyde is also emitted into the atmosphere from biomass burning [*Lee et al.*, 1997], industrial fugitive gas emissions, and emissions from vegetation [*Carlier et al.*, 1986, and references therein]. In the remote atmosphere, by contrast, methane (CH_4) oxidation becomes the dominant source of this gas.

[3] In addition to its reaction with OH (R1), CH_2O decomposes via two different photolysis channels, (R2a) and (R2b), which depend upon wavelength [*Calvert et al.*, 2000].

$$\text{(R1)} \qquad CH_2O + OH \rightarrow HCO + H_2O$$

$$\text{(R2a)} \qquad CH_2O + h\nu(\lambda < 337\ \text{nm}) \rightarrow HCO + H$$

$$\text{(R2b)} \qquad CH_2O + h\nu(\lambda < 365\ \text{nm}) \rightarrow H_2 + CO.$$

In the lower atmosphere, the radical products HCO and H generate the hydroperoxy radical HO2 via (R3) and (R4):

$$\text{(R3)} \qquad HCO + O_2 \rightarrow HO_2 + CO$$

$$\text{(R4)} \qquad H + O_2 + M(N_2, O_2) \rightarrow HO_2 + M(N_2, O_2).$$

The radical photolysis channel (R2a) followed by (R3) and (R4) is a net source of odd hydrogen radicals, HO_x, (HO_x = HO_2 + OH + H) in the atmosphere. This radical channel plays a larger role in HO_x production for high solar zenith angles [*Fried et al.*, 1997b] and in the mid to upper troposphere where radical production from $O(^1D)$ with H_2O diminishes as the available H_2O vapor decreases with altitude [*Wennberg et al.*, 1998].

[4] As many hydrocarbon reactions initiated by OH, O_3, and/or Cl involve CH_2O as an intermediate, CH_2O represents an important test species in evaluating our understanding of the mechanistic details of tropospheric chemistry. According to *Crawford et al.* [1999], CH_2O can be twice as sensitive as HO_x to changes in precursor species, making it an ideal candidate for testing the presence of additional HO_x sources in the upper troposphere. Measurement-model comparisons of CH_2O have a rather long history, particularly in air masses thought to be remote where CH_4 oxidation is the primary CH_2O precursor. Such comparisons have exhibited both positive and negative deviations, as well as good agreement. In marine boundary layer air, models both overpredict CH_2O observations [*Lowe and Schmidt*, 1983; *Jacob et al.*, 1996; *Liu et al.*, 1992; *Zhou et al.*, 1996] as well as underpredict observations [*Weller et al.*, 2000; *Ayers et al.*, 1997]. In the middle and upper troposphere, models generally tend to underpredict CH_2O observations [*Jaeglé et al.*, 2000; *Heikes et al.*, 2001; *Fried et al.*, 2002; *Frost et al.*, 2002]. In some cases [*Jaeglé et al.*, 2000; *Ayers et al.*, 1997] new CH_2O production mechanisms have been postulated to explain model underpredictions. The two recent studies by *Fried et al.* [2003] during the TOPSE 2000 airborne campaign and the shipboard studies by *Wagner et al.* [2002] during the 1999 INDOEX campaign are two exceptions to the above tendencies. In both cases observations and model calculations were found to be in good agreement on average. Clearly, our current understanding of the CH_2O budget in the remote atmosphere is far from complete. The interested reader is referred to *Heikes et al.* [2001], *Fried et al.* [2002], *Frost et al.* [2002] and *Wagner et al.* [2002] for comprehensive overviews of these comparisons.

[5] The Transport and Chemical Evolution Over the Pacific study (TRACE-P), which was carried out (February–April) in 2001 over the Pacific Ocean, provided an additional opportunity to study CH_2O measurement-box model relationships over a wide range of longitudes (California to Hong Kong), altitudes ($\sim$0.2 km to $\sim$12 km), and air mass conditions. In addition, we examine in this study measurement and model variance as well as the effects of clouds and marine aerosols on CH_2O concentrations.

2. Methods

2.1. Tunable Diode Laser Measurements of CH_2O

[6] During TRACE-P there were two independent measurements of CH_2O on the DC-8 aircraft, a coil enzyme method employed by *Heikes et al.* [1996] and the tunable diode laser absorption spectroscopic (TDLAS) measurements employed by our group [*Fried et al.*, 2003]. *Eisele et al.* [2003] presents a discussion of the measurement comparison between these two instruments, and this will not be further discussed here. Since the TDLAS system reported twice the number of CH_2O measurements (53% data coverage) as the coil enzyme system (26% data coverage) during TRACE-P, the present study only employs the more extensive 1-minute TDLAS data set, which is tabulated in the official 1-minute averaged merged data set (publicly available at http://www-gte.larc.nasa.gov).

[7] The airborne TDLAS employed during TRACE-P has been described in detail by *Fried et al.* [2003] and *Wert et al.* [2003], and only a very brief description will be presented here. Infrared (IR) radiation (3.5-μm, 2831.6 cm^{-1}) from a liquid-nitrogen cooled lead salt diode laser was directed through a multipass astigmatic Herriott cell (Aerodyne Incorporated), which achieved a total optical pathlength of 100 m in a 3-liter sampling volume, and ultimately onto IR detectors. Data were acquired using second harmonic detection coupled with sweep integration, as discussed by *Fried et al.* [1998]. Sample air was continuously drawn through the Herriott cell at flow rates $\sim$9 standard liters per minute (sLpm) using a heated PFA Teflon line (1.3 cm OD), which protruded outside the aircraft boundary layer and faced perpendicular to the aircraft flow. A winglet structure external to the aircraft allowed us to heat the inlet line to $\sim$35°C to within a few cm of the inlet entrance as well as add zero air to nearly the entire inlet. With the exception of this small inlet section, the entire inlet/sampling cell (inlet volume $\sim$0.13 standard liters) was heated to approximately this same temperature.

[8] As discussed by *Fried et al.* [2003], the 2831.6 cm^{-1} line is free from all known spectroscopic interferences with the exception of methanol. A weak methanol line approx-

imately +0.005 cm^{-1} from the CH_2O feature has been measured in the laboratory by D. Richter (private communication, 2000), and this feature produces a positive interference of 3.8% on the retrieved CH_2O results [*Fried et al.*, 2003]. All CH_2O measurements were corrected for this interference using methanol measurements acquired onboard the DC-8 during TRACE-P.

[9] Zero air was generated onboard the aircraft employing a heated Pd/Al_2O_3 scrubber, which very effectively removes CH_2O without significantly affecting the ambient water vapor concentration. During background acquisition, the zero air flow was re-routed and reintroduced back into the inlet line a few centimeters from the tip at flow rates ~2- to 3-sLpm higher than the total inlet line flow. As discussed by *Fried et al.* [1998], background spectra thus acquired approximately twice every 1.5 minutes, very effectively captures and removes optical noise as well as the effects of sample line outgassing. In fact laboratory measurements under a variety of relative humidities, temperatures, and sampling pressures, indicate accurate CH_2O retrieval using this approach [*Wert et al.*, 2002]. For calibration purposes, standards were generated using a pressure controlled CH_2O permeation system, the output of which was periodically added to zero air in the main inlet line and/or on top of ambient air to check for inlet line losses. The absolute calibration of this system was determined employing a variety of techniques [*Fried et al.*, 1997a, 2002; *Gilpin et al.*, 1997], and based upon the collective calibrations, we estimate a total calibration uncertainty of ±12% at the 2σ level. Small additional terms, including uncertainty in correcting for the small (3.8%) methanol interference, raise the total uncertainty estimate to 13%–15%. We report an individual systematic and total uncertainty for each 1-minute data point.

[10] The measurement limit of detection (LOD) was determined for each 1-minute data point at the 2σ level based upon the replication precision of ambient measurements near the instrument background. A composite of all 1-minute TRACE-P measurements indicated that our 2σ LOD typically fell within the 50 to 80-pptv range and produced a median value of 66 pptv. In all cases ambient 1-minute averages are reported, even those below the LOD as well as negative values. This allows one to average the data further to obtain a meaningful number with a lower LOD under the proper circumstances, and this will be further discussed in a later section.

2.2. Photochemical Box Model

[11] All model simulations of the present study were carried out using the NASA Langley box model of HO_x-NO_x-CH_4 gas phase chemistry [*Crawford et al.*, 1999; *Olson et al.*, 2001; J. R. Olson et al., manuscript in preparation]. The model input was constrained by the observations acquired on the DC-8 aircraft. The official 1-minute averaged merged data set (publicly available at http://www-gte.larc.nasa.gov) was employed for this purpose, and the model results were output on this 1-minute time base. Calculations were only run where measurements of O_3, CO, NO, dew/frost point temperature, and the photolysis frequencies were available. Measurements of NMHCs, which represent a critical input in modeling CH_2O, were available for ~53% of the DC-8 1-minute merged data, and this overlapped ~43% of the data where CH_2O measurements were available. To extend this overlap, NMHC measurements were either interpolated by averaging consecutive measurements (if the data gap was less than 5 minutes), or the nearest measurement was employed for longer gaps. This extended overlap, however, is achieved at the expense of the potential introduction of noise in the model results in some cases.

[12] In addition to the critical inputs described above, model calculations were also constrained by H_2O_2, CH_3OOH, HNO_3, and PAN when measurements were available; otherwise, the model calculated these species. Measurements of oxygenated hydrocarbons (i.e., acetone, methyl ethyl ketone, methanol, and ethanol) were also used to constrain the model when available. Sensitivity of CH_2O to these species was found to be small in the lower troposphere (~10–20%), but at altitudes above 8 km, the potential dominance of oxygenates required that missing values be inferred based on correlation with CO. With the exception of NO, constraining parameters were assumed to remain constant over the diurnal cycle. NO was allowed to vary diurnally while total short-lived nitrogen ($NO + NO_2 + NO_3 + N_2O_5 + HONO + HNO_4$) was held constant. The amount of short-lived nitrogen was determined by matching the modeled NO concentration to the measurement at the appropriate time of day. Model-calculated species (e.g., OH, HO_2, CH_2O, and other radical species) were assumed to be at steady state, meaning that concentrations were integrated in time until their diurnal cycles no longer varied from day to day.

[13] The model did not include any heterogeneous and/or cloud chemistry nor halogen production (Cl + alkane reactions) and destruction (Br + CH_2O) reactions. Dry deposition loss of CH_2O and other soluble species was invoked for data below 1 km at a constant value of 1.0×10^{-5} s^{-1} (1.2 cm s^{-1} deposition velocity and lifetime of 1.2 days). A more detailed discussion of the box model along with the specific rates employed is given by *Crawford et al.* [1999].

2.3. Impact of Box Model Assumptions

[14] Olson et al. (manuscript in preparation) discuss the impact of box model assumptions. However, it is useful to summarize these findings here in terms of CH_2O. First and foremost, the veracity of CH_2O box model calculations critically depend upon the validity of the steady state assumption, which in turn depends upon CH_2O lifetime and the presence of strong localized sources and sinks of CH_2O within its lifetime. During TRACE-P the median CH_2O instantaneous lifetime was 2.2 hours (83% of data with a lifetime <4 hours), and hence in the absence of such localized perturbations, the steady state assumption should be valid. In the presence of localized perturbations from large fresh anthropogenic emissions of NMHC precursors of CH_2O, for example, the steady state assumption will progressively breakdown as the ambient CH_2O concentration depends increasingly on short-lived hydrocarbon precursors. Since there are numerous NMHC precursors of CH_2O, there is also the possibility that unmeasured NMHCs might become important in CH_2O production. While measurements of short-lived NMHCs (e.g., ethene) are available for use in model calculations, these species are oxidized too rapidly for a steady state condition to be established; thus the

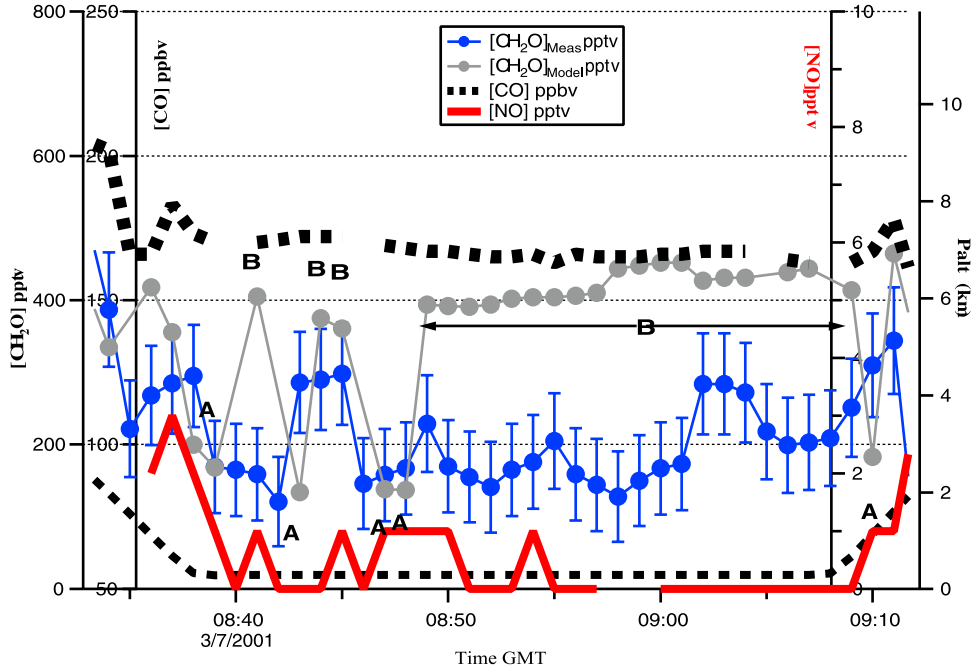

Figure 1. A lower marine troposphere flight leg (flight 7 in the WP region) where one encounters the CH_3OOH problem discussed in the text. Points labeled by "A" employed measured CH_3OOH in the model calculations of CH_2O, while those labeled by "B" employed the modeled CH_3OOH in these calculations. The 1-minute CH_2O measurements are given in blue along with the total measurement uncertainty (2σ level), while the gray points show the modeled values.

model naturally underpredicts the true impact of these short-lived precursors. For most of the TRACE-P data, such species play a negligible role in determining CH_2O concentrations, but they do become significant in fresh emissions.

[15] As shown by *Crawford et al.* [1999], the steady state assumption for CH_2O can also be disturbed by temporal variations of longer-lived precursors like CH_3OOH and NO. The CH_2O production rate is very dependent upon the NO concentration, which influences the production rate for RO radicals ($NO + RO_2 = NO_2 + RO$), which in turn react with O_2 to produce CH_2O. Hence large spikes in NO from urban, ship, lightning, and/or aircraft plumes, will invalidate steady state. Further disagreement can arise from missing processes such as uptake of CH_2O on aerosols and/or in clouds. Since these processes are not simulated in the model they will produce model overestimations.

[16] Two additional model limitations discovered during the course of this study involved instances (N = 466 points, 10% of data) where measurements of key CH_2O precursors like peroxy acetyl nitrate (PAN) (which forms CH_2O via its decomposition through the peroxy acetyl radical) and CH_3OOH were not available and the calculated model values were significantly elevated relative to measurements carried out close in time. While the 466 points in question do not impart a significant effect on the overall CH_2O measurement-model comparison, they cause additional model variance and complicate the interpretation of some horizontal flight legs (to be discussed).

[17] In the case of CH_3OOH, we have identified suspect model points, primarily below 2 km in the lower marine troposphere at very low concentrations of NO less than ~5 pptv. In these cases since the CH_3O_2 + NO channel is effectively turned off, the model calculates fairly high CH_3OOH values. While this is expected, the points in question employ CH_3OOH calculations that are significantly elevated (factor ~2 to 3) relative to measurements close in time. Given the low NO_x environment, the dominate source of CH_2O is the degradation of CH_3OOH, thus in these cases accurate constraint of CH_3OOH in the model becomes critical. Figure 1 illustrates an example of this near the ocean surface. The NO concentration (red solid line) throughout this flight leg was <1 pptv and the CH_2O measurement (blue solid points) and model (gray solid points) comparison points labeled by "B" represent points where only model CH_3OOH was available, while points labeled with "A" employed measured CH_3OOH values in the model. As can be seen, in all cases employing measured CH_3OOH (190 to 220 pptv) the modeled CH_2O was equal to or less than the measurements, and in three of the four cases the measured and modeled CH_2O were in close agreement. By contrast, employing the modeled CH_3OOH (average value 1775 pptv), the modeled CH_2O in 20 out of the 22 comparisons was significantly higher than the measurements. It is also important to note that the modeled CH_2O jumps from one set of values to another based on the CH_3OOH input. The modeled production of CH_2O follows reaction (R5), which produces CH_3OOH at low NO concentrations with HO_2 levels of 4 pptv:

$$\text{(R5)} \qquad CH_3O_2 + HO_2 \rightarrow CH_3OOH + O_2.$$

Methyl hydrogen peroxide thus produced decomposes via OH and photolysis to produce CH_2O. It is clear from

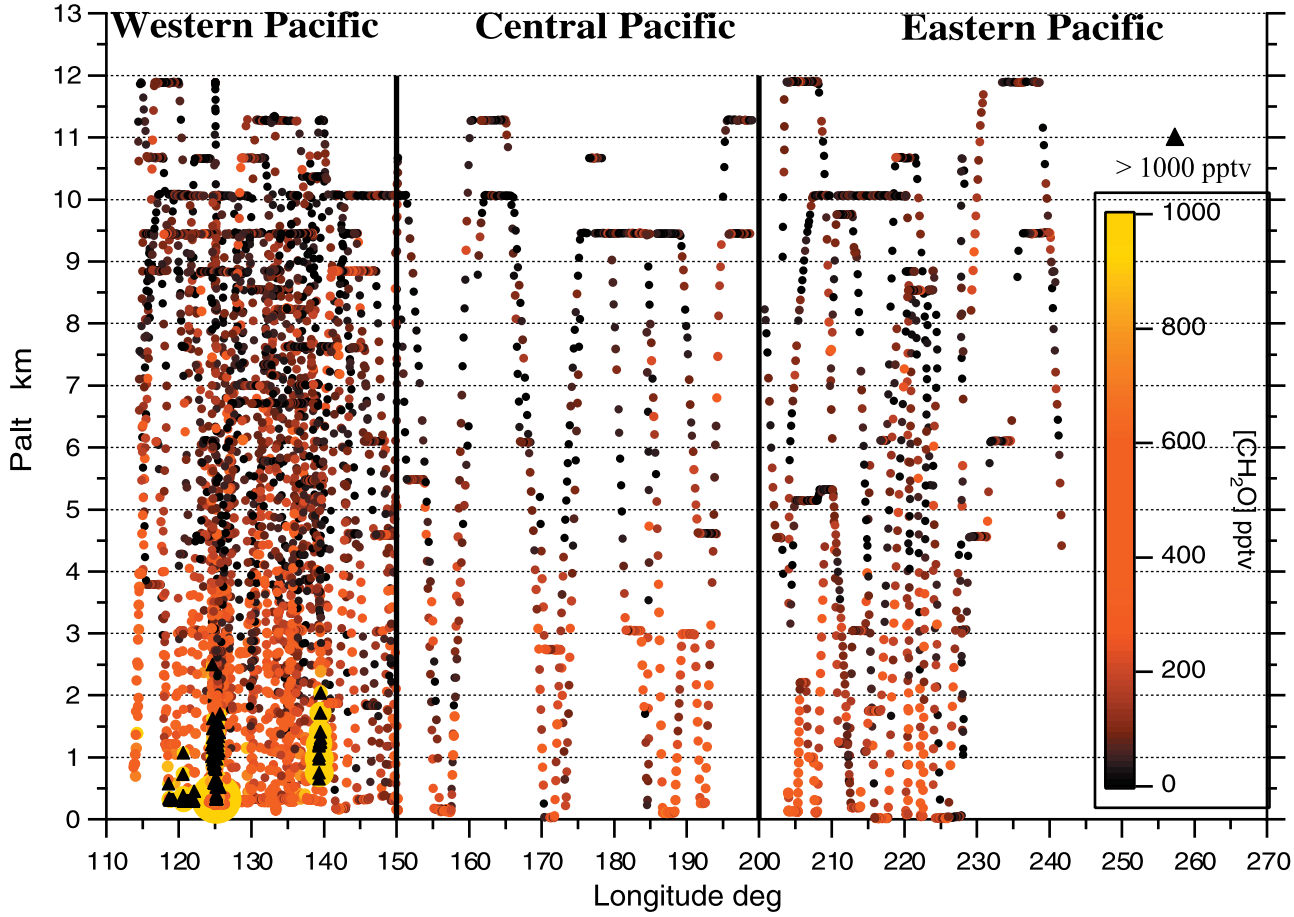

Figure 2. All the 1-minute CH_2O measurements as a function of Palt (km) for the three longitude bins.

Figure 1 that the modeled CH_3OOH values, and hence the modeled CH_2O values, are erroneously high and cannot be trusted in assessing CH_2O in the lower marine troposphere. However, what isn't clear is the cause for the low measurements of CH_3OOH. Can uptake of CH_3OOH be important here or are there self-reactions of CH_3O_2 that do not produce CH_3OOH or CH_2O? In the summary of radical reactions by *Tyndall et al.* [2001], the CH_3O_2 self reaction proceeds via two major channels:

$$\text{(R6a)} \quad CH_3O_2 + CH_3O_2 \rightarrow CH_3O + CH_3O + O_2 \quad (\sim 40\%)$$

$$\text{(R6b)} \quad \rightarrow CH_2O + CH_3OH + O_2 \quad (\sim 60\%)$$

[18] According to *Tyndall et al.* [2001], the yield of other product channels like CH_3OOCH_3 is <6%. Thus there remains an inconsistency between the measured and modeled CH_3OOH and CH_2O in this as well as other legs where NO levels are extremely low. Perhaps reactions of CH_3OOH and CH_2O on aerosols and/or with halogens may be important here?

[19] In the case of PAN, points have been identified where adjacent 1-minute model calculations of CH_2O relied on model PAN values for one or both CH_2O results, and the model CH_2O results differed by more than 100 pptv. While this screening removed some legitimate points in large pollution events where adjacent measured concentrations also changed significantly, this procedure primarily affected erroneous model calculations; the median absolute CH_2O value for adjacent measurement and model differences for the points in question were 61 and 147 pptv, respectively and a maximum model difference of 1811 pptv was observed in one case. The 466 points in question due to missing CH_3OOH and/or PAN have been removed from our analysis.

3. CH_2O Distributions During TRACE-P

[20] Figure 2 shows all 1-minute airborne TDLAS measurements of CH_2O acquired during TRACE-P as a function of altitude segregated into three longitude bins and colored by the CH_2O measurements. These bins reflect the proximity to the Asian source region, and were selected with the aid of the ambient CH_2O observations. Since the highest concentrations tend to be overemphasized in this plot, it is useful to display individual flight legs where the CH_2O measurements are elevated. A value of 500 parts-per-trillion by volume (pptv) was chosen for this purpose. In later discussions, we will show that model-measurement agreement exhibits a distinct deviation for CH_2O > 500 pptv.

[21] The western Pacific (WP) bin had the greatest prevalence of CH_2O observations >500 pptv throughout the lower troposphere, and in many cases levels >1000 pptv. By contrast, the central and eastern Pacific longitude bins (CP and EP) had significantly lower levels at altitudes

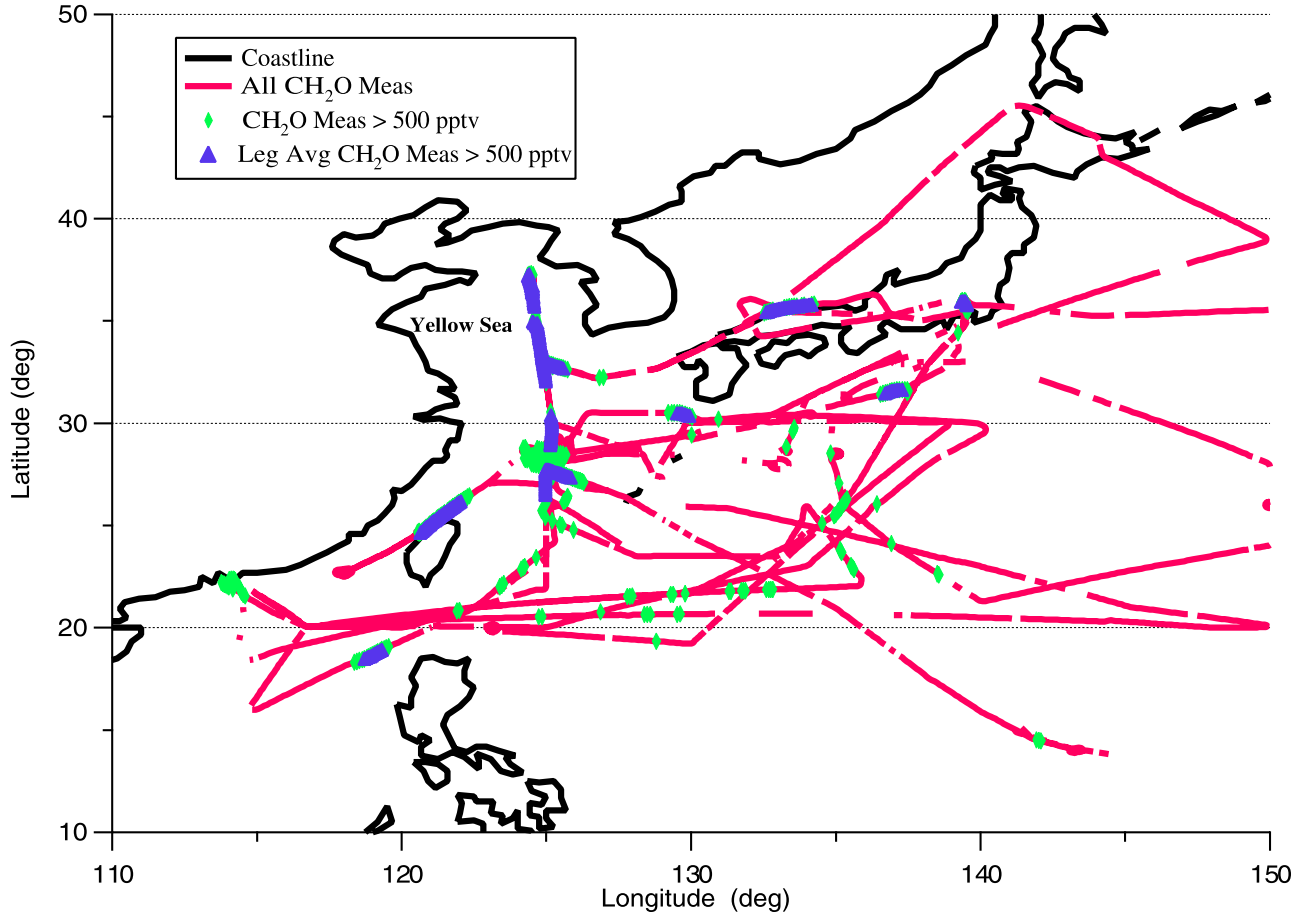

Figure 3. All the western Pacific 1-minute CH_2O measurements as a function of location relative to the Asian coastline. Instantaneous measurements >500 pptv and measurements where an entire horizontal flight leg was >500 pptv are also shown. Measurements in the Yellow Sea show the largest sustained periods where the measurements were >500 pptv.

<5 km, consistent with a median TRACE-P CH_2O lifetime of 2.2 hours and distance from Asian sources. Although latitude typically plays some role in determining ambient CH_2O levels, it was not considered explicitly in the present study, since proximity to the Asian source region plays a more dominant role. We display in Figure 3 all the 1-minute CH_2O measurements in the western Pacific region along with periods where single observations exceeded 500 pptv. We also show in Figure 3 entire horizontal flight legs where the CH_2O observations averaged >500 pptv. Eleven such horizontal flights legs were observed (124 total horizontal flight legs) on 5 different flight days at altitudes <2km, thus indicating the prevalence of elevated CH_2O in the western Pacific region. As shown in Figure 3, most of the elevated CH_2O measurements were observed in the Yellow Sea. In fact, the highest leg average (4097 pptv) and individual 1-minute measurement (10,080 pptv) were observed at the base of the Yellow Sea on flight 13 from a plume directly emitted from Shanghai, China. Analysis of back trajectories show that these air masses were within 0.6–1.5 days downwind of the coast, and in all cases about 12 hours of this transport time was in darkness. It is important to note that Figures 2 and 3 reveal that elevated CH_2O levels >500 pptv were observed at altitudes up to ~2.5 km at longitudes as far east as 140°.

[22] Figure 4 displays the 1-minute CH_2O measurements and time-coincident box model calculations (N = 4006) for the three longitude bins in four different altitude ranges as histograms. Unless otherwise stated, all measurement-model comparisons hereinafter refer to 1-minute time-coincident data where the PAN and CH_3OOH problems discussed previously have been removed and all measurement values (including those below LOD and negative values) are used in the calculation of mean and medians. All the comparison points are shown with the exception of 13 points with measured concentrations >2000 pptv in the western Pacific 0 to 2 km bin. These highly elevated measurement and model results, which represent <1% of the comparison points for this bin, are, however, included in the statistics, which are shown for each altitude range. The 0 to 2 km western Pacific measurement and model distributions shown in Figure 4a reinforce the observations noted in Figure 2; namely that elevated CH_2O levels >500 pptv are mainly limited to the western Pacific 0 to 2 km altitude bin; 37% of the measurements and 22% of the model points fall into this category. As can be seen by the statistics of Figure 4, there is very good agreement between the median measurements and model calculations; most of the differences are <30 pptv, with the largest difference (71 pptv) occurring in the 0 to 2 km central Pacific region. Even in the

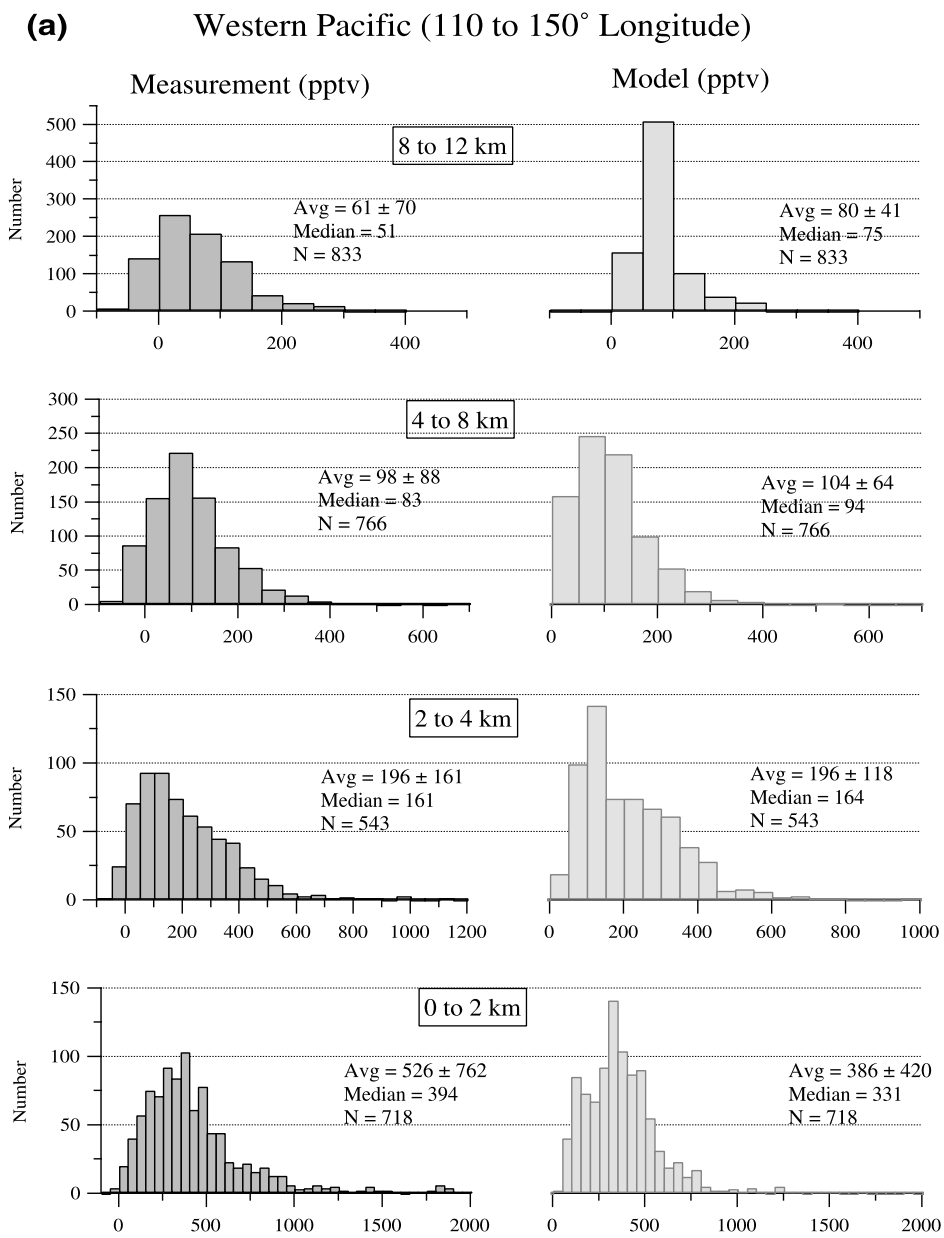

Figure 4. Altitude binned measurement and model histograms for time coincident 1-minute CH_2O data (N_{total} = 4006 points) in three longitude bins.

0 to 2 km western Pacific bin, where the highest CH_2O levels were observed, the medians only differed by 63 pptv. However, as will be discussed, comparisons based upon finer altitude bins revealed some discrepancies in the western Pacific 0 to 2 km bin, which Figure 4a tends to mask.

[23] A comparison of the measurement and model bin standard deviations of Figure 4 indicates that measurements exhibit greater distributions widths than model calculations, with differences being minimized in the 2–4 km range. The PEM-tropics study by *Heikes et al.* [2001] also notes extra measurement variance. In the sections that follow, we will examine this aspect in further detail along with additional measurement-model comparisons based upon comparisons from point-by-point, model bin averages, and horizontal flight leg averages.

4. Measurement Box Model Comparisons

[24] Figure 5 displays median CH_2O measurement and box model results for the entire TRACE-P mission parsed into the three longitude bins and the following altitude steps (0–0.5, 0.5–1, 1–2, 2–4, 4–6, 6–8, 8–10, and 10–12 km). The number of comparison points is given with each altitude range. Of the 4006 comparison points 71% fall into the WP, 14% into the CP and 15% into the EP bins. All three longitude-altitude profiles show a fall off in CH_2O with altitude, as expected due to a decrease in CH_2O precursor

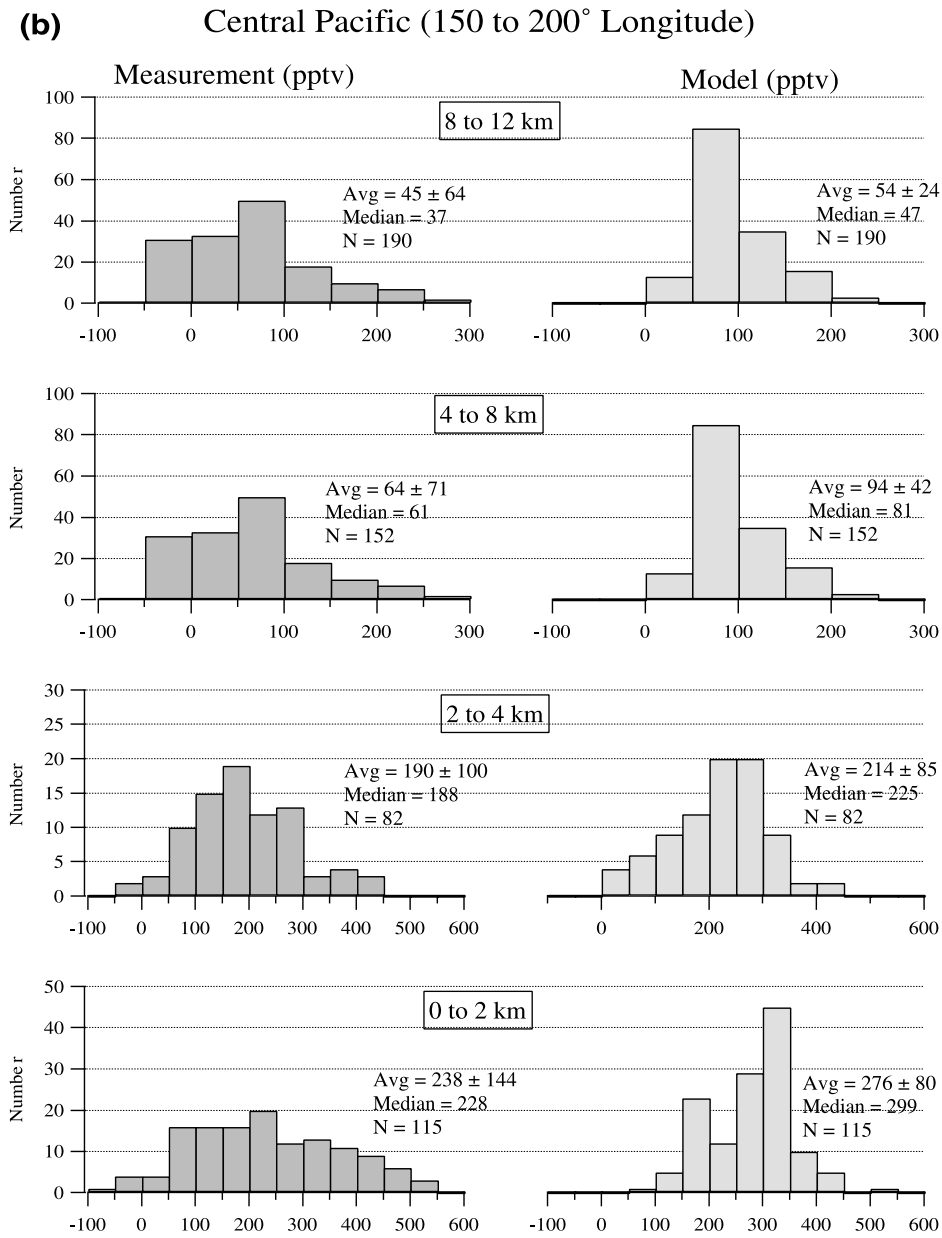

Figure 4. (continued)

concentrations and production rates and a consequent increase in photolysis decomposition rates with altitude. The WP bin shows the steepest altitude gradient due to the proximity to sources of CH_2O and its precursors at the lower altitudes. The upper tropospheric distributions do not change significantly with longitude. At altitudes >2.5 km, where only 0.9% (N = 34) of the combined TRACE-P CH_2O measurements are >500 pptv, Figure 5 reveals excellent agreement between the median measurement and model CH_2O concentrations; the (measurement-model) differences of bin medians range between −37 and 12 pptv. In the WP at altitudes <1 km, where CH_2O measurements are as high as 10,080 pptv, the box model clearly does not capture the magnitude of the highest pollution events. By contrast, in the three lowest altitude bins for the CP (altitude $\leq$ 2 km), where the maximum measurement is 536 pptv, the box model persistently overestimates the observations. While these CP bins are the least robust in terms of number of comparisons, this behavior is suggestive that uptake of CH_2O in the lower marine troposphere (LMT) may be important and this will be further discussed in a later section. This same behavior is not evident in the EP longitude bin for the three lowest altitudes in Figure 5. Here, a number of emission tracers and CH_2O precursors, which are listed in Table 1a (to be discussed), are elevated relative to those in the CP bin, and this may possibly mask any CH_2O uptake.

4.1. Measurement-Model Comparisons Using Linear Regression

[25] Linear regressions yield very useful information, but must be used with caution, because one can obtain different

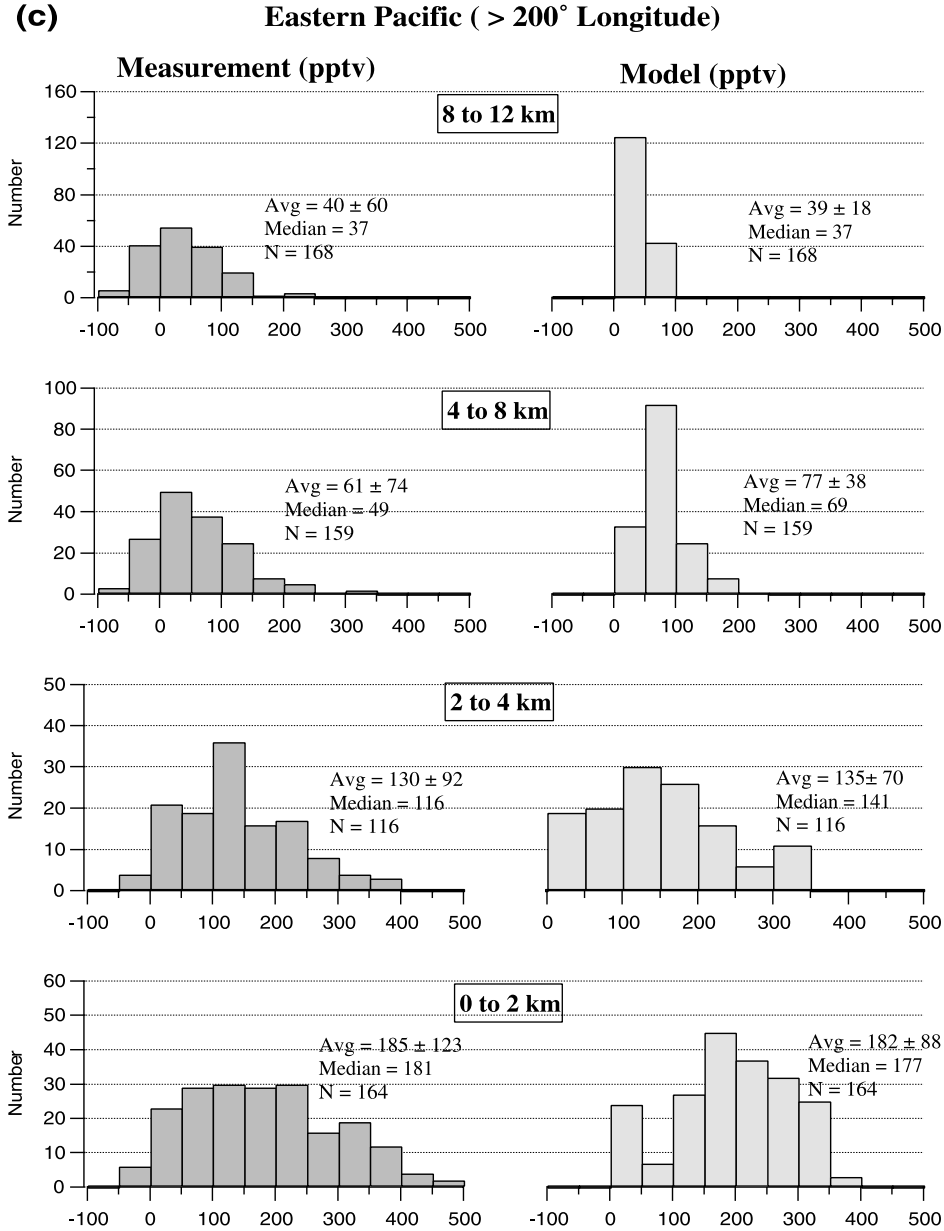

Figure 4. (continued)

results depending upon the data selected to fit and the method of fitting. All regressions of the present study are based upon weighted bivariate fits where the sum-squared perpendicular distances between each point and the fit line are minimized [*Neri et al.*, 1989]. In all cases we employ weights that are proportional to the reciprocal-squared precision estimates for both the measurement and box model calculations. These precisions are the 2σ LODs in the case of the measurements. Drifts of the instrument sensitivity between calibrations is not included in this weighting since it is typically 2 to 3 times smaller than the 2σ LODs for measured CH_2O concentrations less than 1000 pptv (to be discussed); the standard deviation of the calibration sensitivity over the course of a flight or between flights typically ranged between 2 to 3%. For the model calculations we adopt the sensitivity analysis of *Frost et al.* [2002] where the 2σ random model uncertainties were assigned a value of 0.24 times the model concentration. A bivariate fit of the measurements versus the model for all 4006 comparison points yields a slope of 1.52 ± 0.02, an intercept of (−51 ± 3) pptv, and $r^2 = 0.79$. This fit, however, is unduly influenced by 50 extremely high comparison points where the measurements are all >1000 pptv, where the model significantly underpredicts the observations by as much as 5450 pptv and yields a median difference of 875 pptv. Although these results are valid and must be reported, they do not reflect the comparison where 99% of the data reside. Figure 6 displays a scatterplot and bivariate fit where the measurements are limited to values <1000 pptv, and this results in smaller values for the slope (1.38 ± 0.02), intercept (−39 ± 3 pptv), and r^2 (0.57). The reduction in r^2 from 0.79 to 0.57 implies a poorer correlation. However,

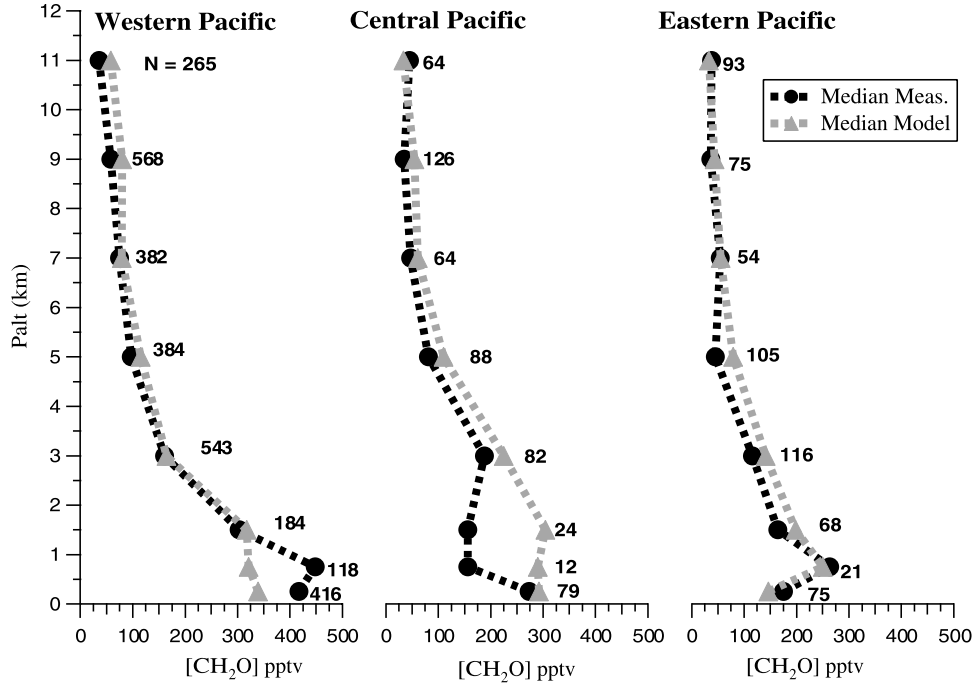

Figure 5. The same data as Figure 4 with the median measurement and modeled CH_2O concentrations plotted in eight different altitude and three longitude bins. The number of points (N) in each bin is shown.

this can be attributed to the reduced dynamic range of the data, and thus one must use r^2 values with caution, particularly in assessing the degree of covariance between measurements and models.

[26] The results of Figure 6 nevertheless indicate a large amount of scatter. However, before this is addressed, it is useful to further examine potential systematic differences between measurement and model results, and one approach toward this end is to calculate measurement averages in model bins [*Fried et al.*, 2003]. Figure 6 displays measurement averages in each 25-pptv-model bin along with the resulting bivariate linear fit up to a model bin value of 450 pptv. At higher model values, the bin averages predominately deviate upward from the linear fit. This same behavior was observed during the TOPSE 2000 study [*Fried et al.*, 2003]; there the onset of nonlinearity occurred at model bin values of 350 pptv. The bin averages of Figure 6 yield a slope of 0.98 ± 0.03, which like the TOPSE study (slope of binned data = 1.14 ± 0.08) is suggestive that there is no systematic bias on average between CH_2O measurements and box model results out to model values ~450 pptv. However, as in TOPSE, the model results progressively underpredict the observations at higher concentrations. This is consistent with the breakdown of the steady state assumption for fresh emissions. We believe that this effect is responsible for the nonzero intercept (−39 ± 3 pptv) in the linear fit for the 3956 data points of Figure 6. Points larger than ~450 pptv both raise the slope and increase the negative intercept. Like the binning approach, restricting the linear fit for the individual 1-minute original comparisons to values less than 450 pptv results in a near-unity slope (1.02 ± 0.03) and a near zero intercept (−9 ± 3 pptv).

[27] What is somewhat surprising, however, is the fact that there is still a great deal of scatter for individual 1-minute comparisons in the 200 to 450 pptv model range where the assumption of steady state should be valid and the measurements are >6 times the 1σ detection limit. Figure 7 further addresses this issue by displaying (measurement-model) differences as function of model values with points color-coded and sized by the concentration of the highly reactive alkene, ethene. This plot contains the same data set as Figure 6 (measurements <1000 pptv). Figure 7 displays the combined measurement and model precision estimates at the 2σ level (solid gray curves), which reflects the bounds within which 95% of the (measurement-model) differences should reside if systematic differences are not present. The average difference in Figure 7 for measurements <1000 pptv is 2 ± 116 pptv. Thus, unlike a normal scatterplot, Figure 7

Table 1a. Fresh Emission Tracer Concentrations for the Eight Pressure Altitude Bins[a]

	Eight Pressure Altitude Bins, km							
Tracer	<0.5	0.5–1	1–2	2–4	4–6	6–8	8–10	10–12
CO	156	158	138	204	110	109	174	87
NO	6	5	10	50	20	23	59	30
NO_2	25	29	27	111	23	14	28	8
C_2Cl_4	9.4	9.5	7.9	5.8	4.7	4.9	5.3	2.8
CH_4	1826	1828	1818	1790	1789	1802	1800	1785
Ethane	1785	1847	1501	1313	993	1112	1203	816
Ethene	8	8	5	3	3	3	12	11
Ethyne	449	470	335	533	231	421	528	268
Propane	456	482	336	200	139	141	163	84
Propene	3	3	3	3	3	3	3	3
i-Butane	56	56	36	23	13	16	21	9
n-Butane	86	90	59	38	19	22	30	12
Benzene	96	101	62	99	38	81	97	40

[a]All in pptv except CO and CH_4, which are in ppbv. The tracer concentrations were based on the 3rd quartile values for the central Pacific and the altitude bin in question. The fresh emission label was applied to those horizontal flight legs where the majority of tracer concentrations averaged over the leg exceeded the 3rd quartile limits.

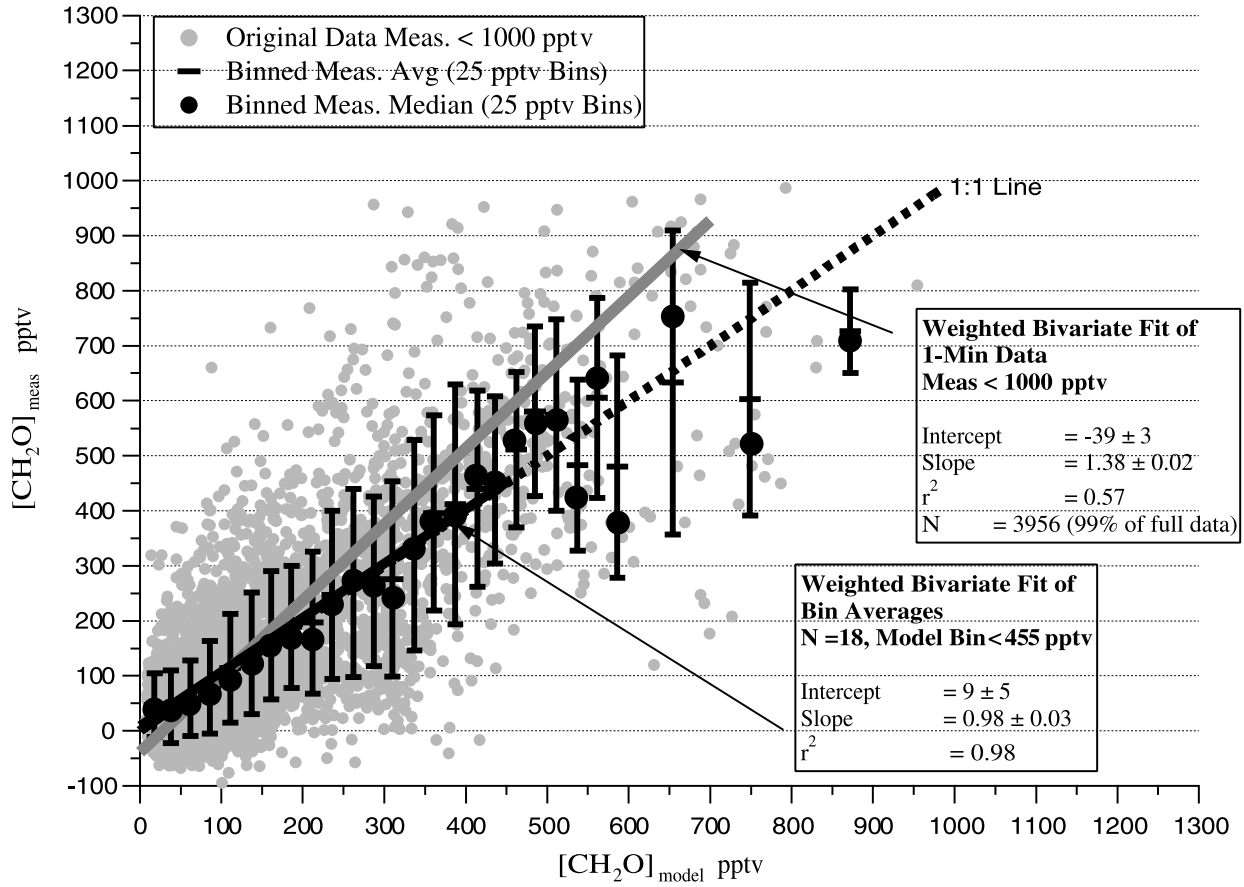

Figure 6. Scatterplot of 1-minute measurement-box model comparisons (light gray points) for measurements <1000 pptv (N = 3956, 99% of the data). The dark solid gray line displays the weighted bivariate fit of these data while the dark solid black line displays a linear fit for the bin-averaged data (dark horizontal lines) Here measurements were averaged in each 25 pptv model bin and the bivariate fitting weights were determined from the bin measurement and model standard deviations instead of the respective precisions. The linear fit was carried out up to a model bin value of 450 pptv.

highlights the component of scatter that one should expect based upon the finite measurement and model precisions. Sixty percent of the measurement-model comparisons fall within the combined precision limits for model values <450 pptv (the limit indicated in Figure 6 where curvature becomes obvious). Clearly, there are still systematic measurement-model differences on the individual 1-minute comparison points, and one such obvious source in Figure 7 is elevated ethene concentration. As can be seen, many of the positive outliers have high ethene concentrations, in many cases >100 pptv and in some cases by as much as 750 pptv. The model input ethene concentrations are too low during such highly elevated pollution events, which in turn results in model underpredictions. Other reactive alkenes like propene would also cause similar problems. For model values <450 pptv, 18% of the Figure 7 outliers have ethene concentrations >20 pptv (the highest median ethene concentration for the less polluted CP and EP regions is 6 pptv).

[28] It is interesting to note that the percentage of positive (19%) and negative outliers (21%) for model values <450 pptv in Figure 7 are nearly equivalent, and this is consistent with the average (measurement-model) difference near zero. However, this implies that the positive perturbation associated with high ethene values must be countered by a negative perturbation from other sources, such as the effects of clouds; many of the large negative outliers of Figure 7 were acquired in clouds, and this will be further discussed.

[29] It must be noted that in Figure 7 not all high ethene points result in measurement-model disagreement. In addition, ethene in many cases may simply be a marker and the real problem may be primary emissions, as suggested by one of the peaks in Figure 8. Data in this plot were acquired at altitudes <2 km in the Yellow Sea where 3-D model analysis indicated mixed plumes (0.25 to 1.5 days old) originating from various cities in China, including Beijing, Taiyuan, Qingdao, and Wuhuan. An examination of back trajectories indicates that these mixed plumes were 15–19 hours downwind of the coast. In addition to measurement and modeled CH_2O concentrations, this plot also includes CH_2O production rates, total production rate, rate from CH_3O_2 + NO, and rate from etheneO_2 (the peroxy radical formed by addition of O_2 to ethene) + NO. As can be seen, production from these two RO_2 + NO reactions account for nearly all the CH_2O production in the model in Figure 8; at 05:13 GMT these two

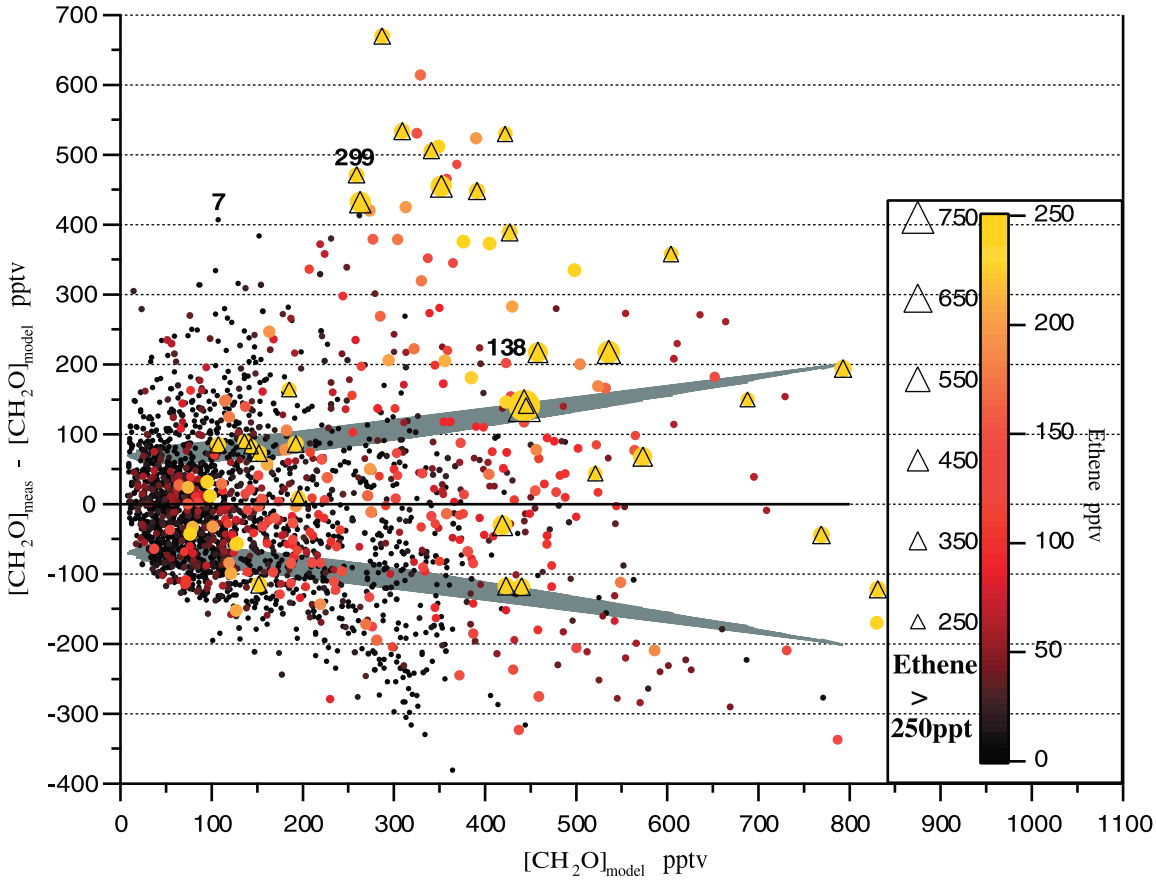

Figure 7. Time coincident (measurement-model) differences as a function of modeled CH_2O and color-coded and sized by ethene. Increasing ethene concentrations up to 250 pptv are denoted by larger circles. Progressively larger open triangles denote higher ethene concentrations >250 pptv. The ethene concentrations (in pptv) are denoted immediately above 3 points to facilitate the assignment of ethene levels. The solid gray curves represent the combined measurement and model precision at the 2σ level.

reactions account for 84% of the total CH_2O production. It is interesting to note that the modulated measured CH_2O (defined by the peak concentration at 05:13 minus the lobe value at 05:09, 505 pptv) is nearly identical to that modeled for the same points (493 pptv), suggesting that the measured structure during this period is faithfully captured in the model by RO_2 + NO reactions. Nevertheless, the measured CH_2O concentration during this period is ~twice that modeled, and these two facts suggest that additional CH_2O from sources other than those related to NO modulation are operative. Simply increasing the CH_2O production rate by increasing the starting ethene concentration to bring the model into agreement with the peak measurements results in incorrect NO modulation depth and a model ethene concentration at the time of measurement that is much too high compared to observations. Since most CH_2O production steps involve NO at some point, it is highly likely that the above observations reflect direct CH_2O emissions. Based on the difference in peak measured and calculated values, these direct emissions would need to account for about 1 ppbv of the observed CH_2O. As noted earlier, given the time downwind from the coast (15–19 hrs) and the time of sampling (near local noon) the observed CH_2O would have only 6–7 hours of sunlight exposure downwind of the coast. Thus, CH_2O near the source could be expected to be in the range of 3–10 ppbv. By contrast to the peak in question, all other peaks in Figure 8 did not exhibit similar evidence for a direct CH_2O emission source.

4.2. Measurement-Model Comparisons in Cloud-Free and In-Cloud Conditions

[30] In assessing the effects of clouds on CH_2O levels and comparisons with box model results, it is important to ensure that CH_2O uptake events are not masked by pollution. This precaution is necessary since both elevated and depressed CH_2O levels may be associated with clouds. On one hand, clouds are often associated with fronts with the consequent transport of boundary layer pollution up into the mid-troposphere. Any uptake in this case could be masked by model underestimations from fresh emission sources. It is also entirely possible that the two processes could balance, resulting in the cancellation of two modeling perturbations. In the absence of these effects in cleaner background air masses, one should observe the uptake of gas-phase CH_2O in clouds, depending upon the exposure time, temperature, liquid water content as well as other parameters [*Barth et al.*, 2003]. The box model simulations by *Barth et al.* [2003] indicate a gas-phase depletion of

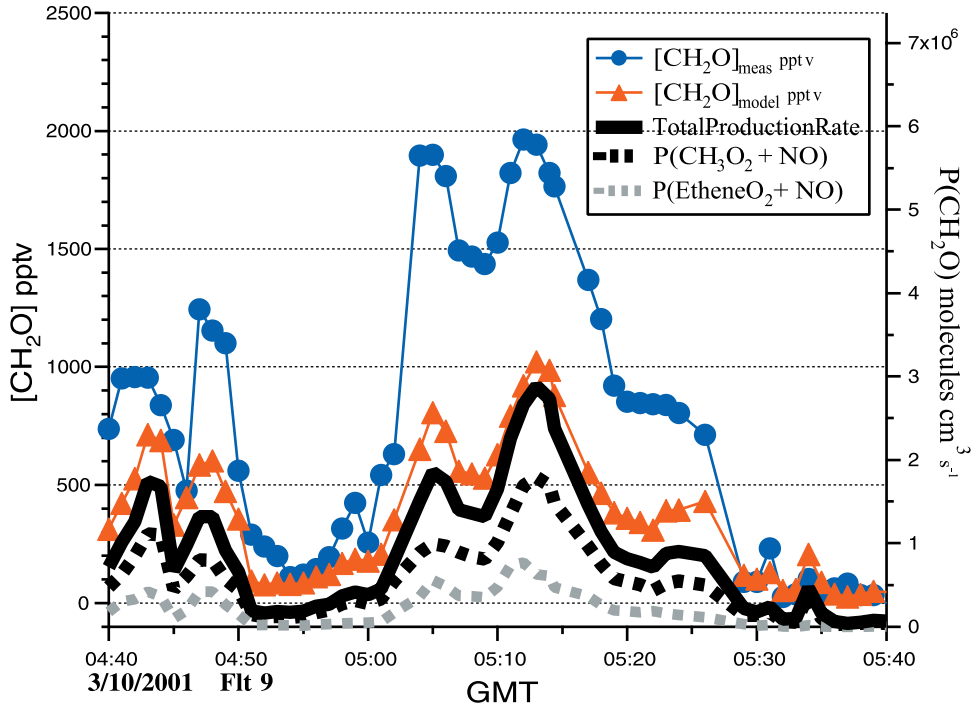

Figure 8. Measurement and model comparisons for data acquired at altitudes <2 km in the Yellow Sea where 3-D model analysis indicated mixed plumes (0.25 to 1.5 days old). This plot also includes CH_2O production rates ($P(CH_2O)$, right-hand axis), total production rate, rate from CH_3O_2 + NO, and rate from $etheneO_2$ (the peroxy radical formed by addition of O_2 to ethene) + NO.

~29% after a half-hour cloud exposure time and a depletion of ~42% after 1 hour (M. C. Barth, personal communications, 2003).

[31] Time periods when the DC-8 was flying through clouds were determined from measurements of aerosol volume density for particles in the 10–20 μm size range in conjunction with the DC-8 videotapes. When the volume density (μm^3 cm^{-3}) for a 1-second data point exceeded a given threshold, the appropriate 1-minute average data was assigned a cloud index depending on the threshold exceeded: (1) haze > 100, (2) intermediate > 800, and (3) cloud > 2000. In the lower marine troposphere (LMT) the haze and intermediate cloud regimes often reflect sea salts under humid conditions and not pure clouds per se. Below 1 km 92% of the in-cloud measurement-model comparisons in the WP regime fall in this category. The LMT comprises what some authors refer to as the buffer layer [*Russell et al.*, 1998] and the underlying marine boundary layer (MBL).

[32] Figure 9a displays the WP measurement-model comparisons segregated into cloud-free and in-cloud conditions. The present analysis is restricted only to the WP region since the number of comparisons for each altitude in the CP and EP regions was too small (maximum = 5). The in-cloud WP data was restricted only to cloud index 3 data where the liquid water content was typically >0.02 g m^{-3} (average = 0.05 g m^{-3} for the 0–6 km range). Figure 9a shows the median measured and modeled CH_2O concentrations as a function of altitude along with the number of comparison points for both cloud conditions as well as the median point-to-point (measurement-model) differences in parentheses. This figure exemplifies the two effects of clouds just discussed. Continental outflow and the consequent model underestimations can be seen in both the in-cloud and cloud-free data between 0 and 1 km. Above 1 km, Figure 9a shows that all in-cloud measurements and model values are higher than corresponding cloud-free values, reflecting the effects of continental outflow in and around clouds. Although the two data sets start to converge above 4 km, the in-cloud data are still elevated relative to cloud-free conditions. However, measurement-model comparisons for in-cloud data relative to cloud-free data in Figure 9a also reveal persistent model overestimations at altitudes above ~1 km, where fresh emissions are less extreme. The biggest disparity occurs in the 4–6 km altitude range where the in-cloud median (measurement-model) difference is −49 pptv compared to −3 pptv under cloud-free conditions, and this amounts to a 24% in-cloud uptake. It is important to reiterate that in all cases measured j values were used in the calculations, thus avoiding calculation errors due to errors in the photolysis frequencies.

[33] Although the above model overestimations are small for the composite WP in-cloud measurements, the complicating nature of fresh emissions in and around clouds cannot be ignored, and as a result the fundamental uptake of CH_2O in clouds may be even larger than those in Figure 9a for cleaner background cases. Figure 9b (flight 13) shows the one example where this was evident during TRACE-P. In this plot we display the measured CH_2O concentrations along with the total 2σ total uncertainties as error bars upon flying in (cloud index 3 only) and out of clouds while ascending from an altitude of 1.6 km to an altitude of 3.7 km southwest of Japan (25° N latitude and 127° longitude). We only highlight in this figure (shaded boxes) those in-cloud measurements where there are at least two continuous in-

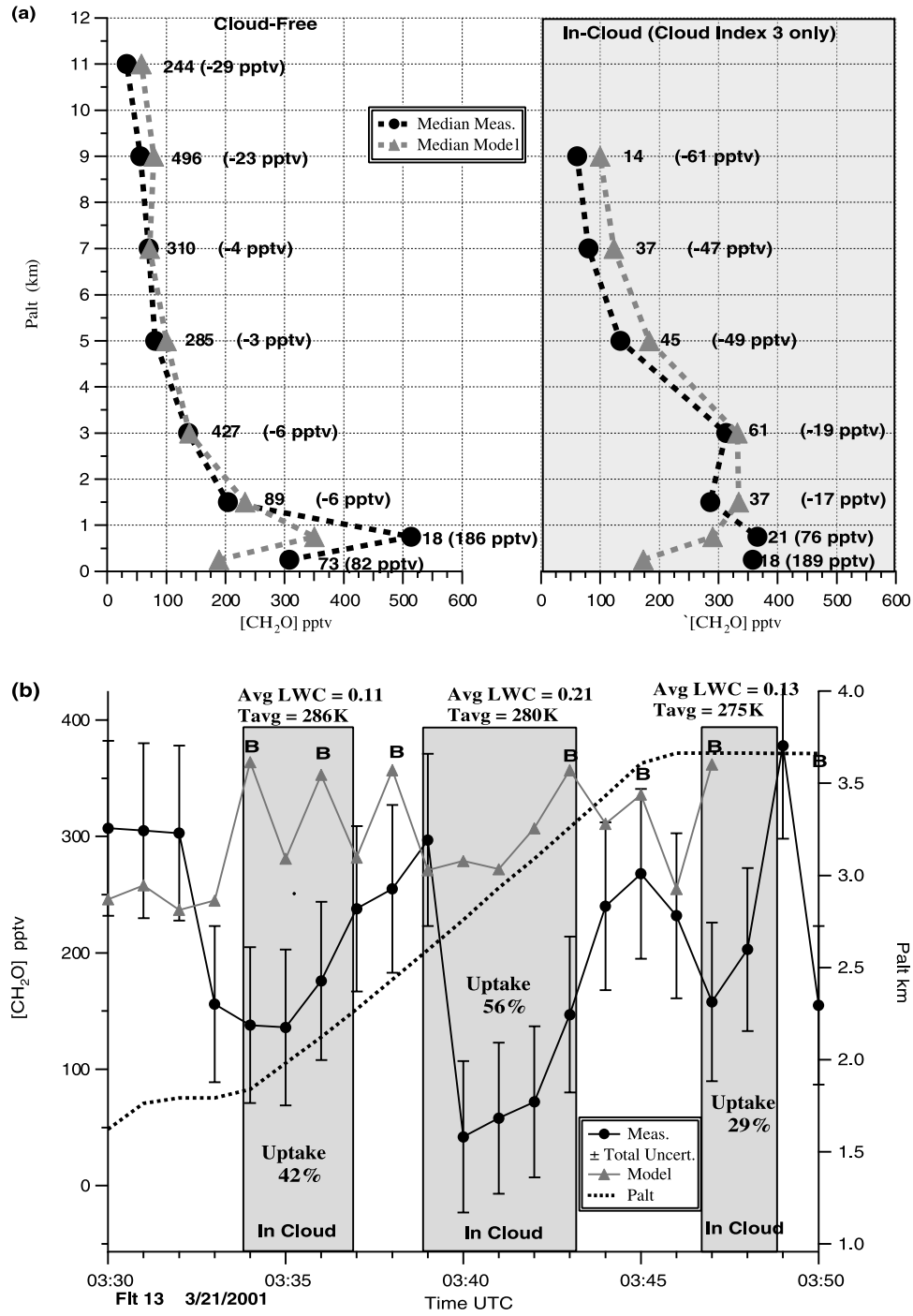

Figure 9. (a) Western Pacific median measurement and model altitude profiles for cloud-free and in-cloud conditions. The number of comparisons is shown along with the point-by-point median (measurement-model) differences in parenthesis. (b) The one example during TRACE-P where: (1) there were at least two continuous in-cloud observations, (2) the liquid water content was at least 0.01 g m^{-3} and the cloud index was 3, and (3) fresh pollution was not evident. The average temperature (Tavg) and liquid water content (Avg LWC in g m^{-3}) are given with each in-cloud segment. Points labeled with a "B" employed model calculated CH_3OOH concentrations in the box model, while all other points employed measured values in the calculation.

cloud observations where the liquid water content (LWC) was at least 0.01 g m^{-3}. The box model results, which are displayed, are further annotated according to the CH_3OOH concentration used in the calculation; as in Figure 1, points labeled with a "B" employed model calculated CH_3OOH concentrations while all other points employed measured values in the calculation. As can be seen, the oscillation between employing measured and modeled CH_3OOH

causes some artificial oscillation in the calculated CH_2O values, as previously discussed.

[34] This calculation oscillation notwithstanding, one observes a depression in the measured CH_2O concentrations relative to model values upon entering each cloud segment. In each case the depressed observations are clearly outside the total measurement uncertainty limits. The largest CH_2O uptake (56%) occurred in the second cloud segment where the liquid water content (LWC) was the largest. Uptake percentages were calculated from the average (measurement-model) difference divided by the average model value in each cloud segment. The (perturbed) modeled "B" points were not included in this calculation. For the first cloud segment, the six nonperturbed model values (3:30–3:37) were averaged (258 pptv). The three in-cloud measurements (3:34 to 3:36) produced an average value of 150 pptv. For the second in-cloud segment, the four nonperturbed model values (3:39 – 3:42) produced an average value of 283 pptv, and this was compared to the five observations (3:39–3:43), which averaged 123 pptv. A peak uptake of 85% was observed at 3:40 during this segment. The third cloud segment only has one nearby nonperturbed model value for comparison (at 3:46, model = 255 pptv), which compares to an averaged measurement value of 181 pptv (3:47–3:48). Although none of the sampling conditions during these cloud uptake events precisely match the conditions employed during the simulations by *Barth et al.* [2003] (altitude = 1.5 km, LWC = 0.3 g m^{-3}, T = 285 K), the comparison point at 03:36 (altitude = 2.1 km, LWC = 0.23 g m^{-3}, T = 285 K) comes the closest. Our measured CH_2O uptake of 32% ((176–258)/258 $\times$ 100) is in the range of Barth's values of 29–42% for 0.5–1 hour of cloud exposure. In fact, all the in-cloud data of Figure 9b fall near this range. However, we have no way of determining in each case how long the sampled air was exposed to clouds.

[35] Despite the fact that the above observations are based upon a limited data set, and we have no information regarding the in-cloud history/exposure time, the present CH_2O observations reveal direct evidence to support model uptake in clouds with only minimal complications caused by fresh pollution. Clearly additional observations of this kind are needed. The results of Figures 9a and 9b clearly point to the contribution of uptake to the scatter in the individual measurement-model comparisons of CH_2O evident in Figures 6 and 7.

5. Horizontal Flight Legs, and Measurement Model Variance

[36] Up until this point our analysis has not explicitly focused on measurement and model variance. Many studies involving CH_2O, such as *Jacob et al.* [1996], *Heikes et al.* [2001] and *Jaegle et al.* [2000] to name a few, note that box model results in general fail to capture the observed variability. Clearly factors that are important in this regard are: (1) measurement imprecision, particularly extra sources of imprecision that may be related to changes in aircraft sampling conditions (i.e., speed, attitude, altitude, cabin and ambient pressures and temperatures); (2) model variability due to uncertainties in critical input values as well as the availability of important constraining species, (i.e., the PAN and CH_3OOH issues raised previously); (3) atmospheric variability not accounted for by model assumptions (e.g., non steady state conditions and cloud uptake).

[37] In this section we further assess measurement and model variance by examining horizontal flight legs. Such legs also allow us to integrate over time periods longer than 1-minute, resulting in an improved measurement precision (to be discussed) and utilization of data at and below the 1-minute limit of detection. A total of 124 flight legs were identified where there were at least 5 minutes of time-coincident measurement and model results where the DC-8 aircraft did not change altitude and where the cabin pressure was constant. The latter is important since cabin pressure changes affect our alignment and hence our measurement precision [*Wert et al.*, 2003]. The average leg duration was 25 minutes in length and typically contained 15 time coincident measurement-model comparison points. By identifying such legs we minimize the factors above, with the exception of natural atmospheric variability that may contribute to measured and modeled CH_2O variance. Horizontal flight legs more typically encounter air masses with similar histories and this minimizes modeling input errors due to incomplete NMHC coverage, which may be missing and/or nonrepresentative during ascents and descents.

[38] Unlike the binning approach presented in section 4.1, horizontal flight leg averages operate on air masses with ostensibly the same history. This minimizes the possibility of masking unique atmospheric processes that may be present over entire flight legs but the number of such observations may be limited relative to the overall number in a given model-averaging bin. The very low temperature measurement-model discrepancies noted by *Fried et al.* [2003] at low model concentrations under dark conditions during TOPSE is one example of this. Thus, horizontal flight leg measurement-model comparisons provide an additional means by which to assess systematic differences. In addition, this approach minimizes many transitory excursions into and out of pollution and cloud layers when changing altitudes.

[39] Of course, large pollution layers and cloud effects may still be encountered during horizontal legs, and such legs were flagged in this analysis. The tracers and their concentrations listed in Table 1a were used to identify fresh emissions for this purpose. We list in Table 1a the 3rd quartile tracer concentrations obtained from the eight altitude bins for the central Pacific longitude region, which should be relatively free of most local sources. Since no single tracer listed is ideal, we used all the tracers; we applied the fresh emission label to those flight legs where the tracer leg average concentration for the majority of tracers was greater than the 3rd quartile tabulations. This resulted in 62 fresh emission flight legs (50% of the flight legs, N = 36 of such legs had cloud encounters over the majority of the leg, N = 24 were cloud-free, and 2 indeterminate cloud status). In contrast to Figure 9a (cloud index 3 only), all cloud encounters (cloud index 1, 2, 3) were employed in this tabulation. Likewise, background legs were identified where the tracer leg average concentration for the majority of tracers was equal to or less than the 1st quartile tabulations of Table 1b. This resulted in 12 flight legs (10% of the horizontal flight legs), which were all in cloud-free conditions at or above 3 km (N = 9 were above 6 km). The measured CH_2O concentration averaged 61 pptv

Table 1b. Background Tracer Concentrations for the Eight Pressure Altitude Bins[a]

	Pressure Altitude Bins, km							
Tracer	<0.5	0.5–1	1–2	2–4	4–6	6–8	8–10	10–12
CO	106	99	105	114	86	81	79	74
NO	1	0.5	2	6	11	12	15	12
NO_2	6	4	9	21	12	8	8	4
C_2Cl_4	3.7	3.3	3.5	4.2	2.9	2.7	2.8	1.2
CH_4	1769	1773	1772	1767	1763	1756	1777	1748
Ethane	675	654	699	825	536	527	502	431
Ethene	3	3	3	3	3	3	3	3
Ethyne	116	117	136	170	80	80	73	50
Propane	43	37	55	80	37	29	32	15
Propene	3	3	3	3	3	3	3	3
i-Butane	3	3	4	6	3	3	3	3
n-Butane	4	3	4	9	3	3	3	3
Benzene	24	23	29	26	12	12	8	3

[a]Same units as in Table 1a. The tracer concentrations were based on the 1st quartile values for the central Pacific and the altitude bin in question. The background label was applied to those horizontal flight legs where the majority of tracer concentrations averaged over the leg was equal to or less than 1st quartile limits.

for these background legs. We also identified an intermediate leg category (N = 50, 40% of the legs) where the majority of tracer concentrations fell in between the two limits of Tables 1a and 1b (N = 7 in-cloud, N = 35 cloud-free, and 8 indeterminate cloud status).

[40] Figure 10 shows a plot of the leg measurement average versus the leg model average for all but one of the 124 horizontal flight legs discussed. The excluded leg falls outside the limits of Figure 10 (leg measurement average = 4108 ± 3044 pptv, leg model average = 2239 ± 1787 pptv). As can be seen, very few of the cloud-free intermediate and background leg averages (N_{total} = 47) exhibit large scatter off the 1:1 line, and a bivariate fit yields a slope of 1.16 ± 0.10 with an r^2 = 0.77. As with the model binning approach, the horizontal flight leg averages reveal no definitive systematic bias between measurement and model results. By contrast, cloud-free fresh emission and in-cloud leg averages show large scatter in both directions from the 1:1 line.

[41] Having identified 35 cloud-free flight legs and a more restrictive set of 12 cleaner background legs where large measurement-model systematic differences have been removed, we now further examine measurement and model

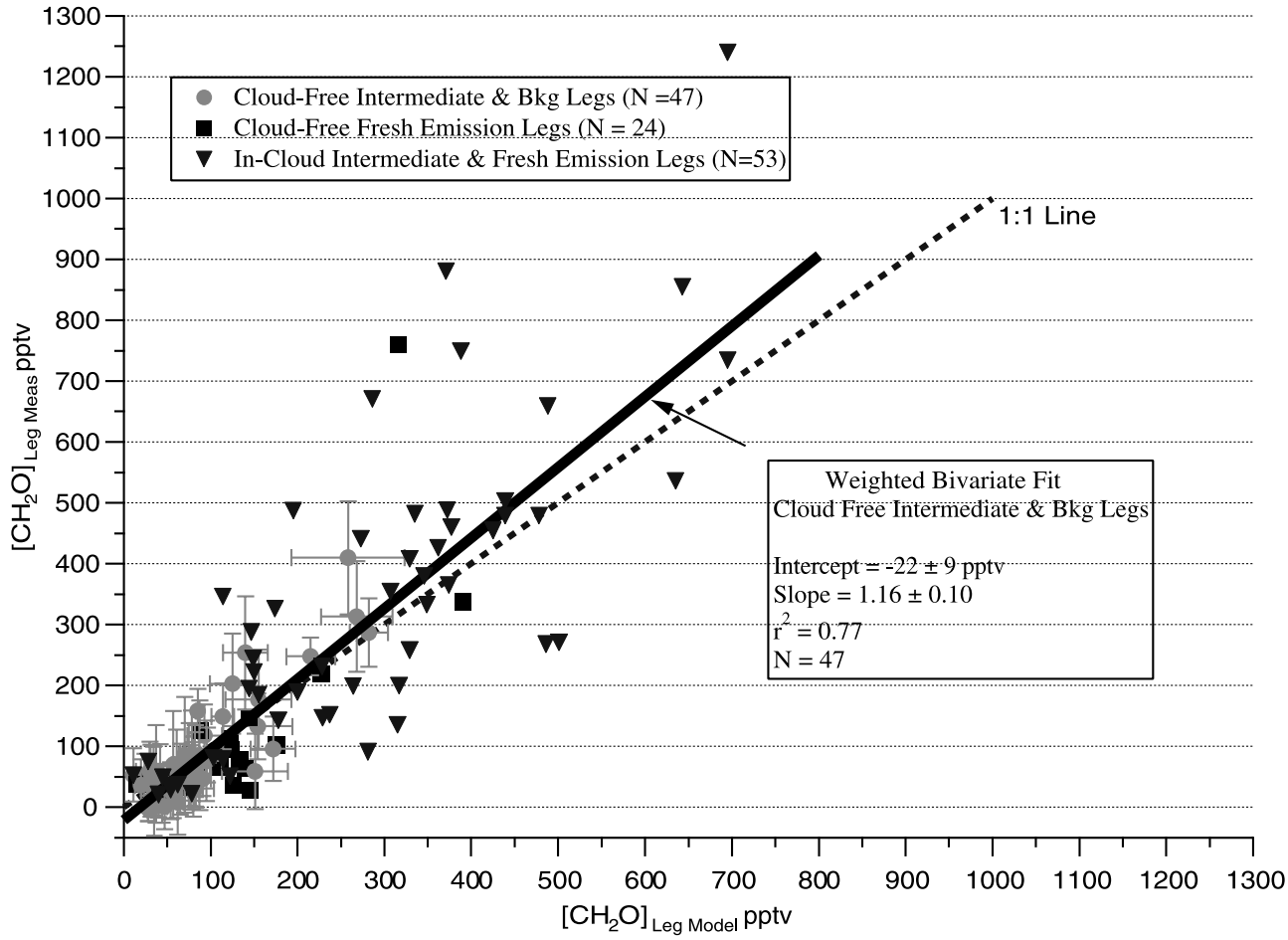

Figure 10. Measurement leg average versus the model average for 123 of 124 horizontal flight legs. The one excluded leg average (leg meas. avg. = 4108 ± 3044 pptv, leg model avg. = 2239 ± 1787 pptv) falls outside the graph window. A total of 47 cloud-free intermediate and background legs were identified (gray points with 1σ standard deviation precisions for error bars, see text for further discussion). The 53 in-cloud intermediate and fresh emission legs also include 10 legs where the cloud status could not be determined.

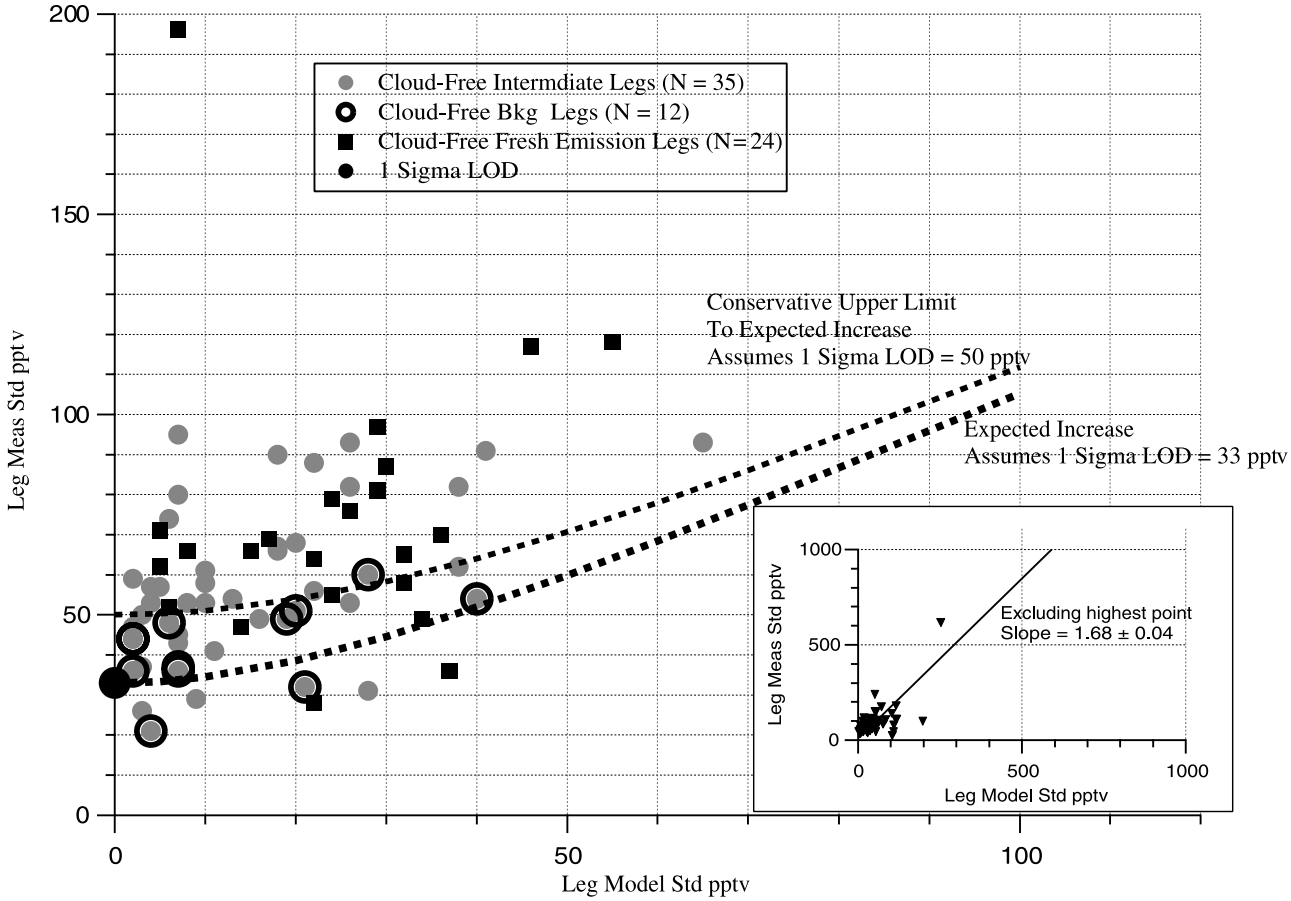

Figure 11. Leg measurement standard deviation versus model standard deviation (σ_{model}) at the 1σ level for each of the 35 cloud-free intermediate legs (gray points) and the more restrictive 12 cloud-free background legs (gray points with large open black circles). The larger filled black circle on the *y* axis represents the overall 1σ measurement LOD (33 pptv). The lower dotted curve was generated from the quadrature addition of the 1σ LOD (33 pptv) with σ_{model}. The upper dotted curve employed a conservative upper limit of 50 pptv for the LOD. Both curves reveal the expected measurement precision for various σ_{model} values. The inset shows this same plot for in-cloud fresh emissions, intermediate and indeterminate cloud status (N = 53).

variance. Measurement (σ_{meas}) and model (σ_{model}) 1σ leg standard deviations were employed for this purpose. This procedure provides a direct assessment of variance without the pitfalls of relying solely on r^2. In Figure 11 we plot the σ_{meas} versus σ_{model} for each of the 35 cloud-free intermediate (gray points) and more restrictive 12 background legs (large open black circles surrounding the gray points). We also show the corresponding points for the cloud-free fresh emission data set (black squares) and the in-cloud data in the inset. The data near the Y-intercept in the main plot (i.e., σ_{model} approaching 0) yield average σ_{meas} results that are close to the 1-minute measurement 1σ LOD (median value = 33 pptv, denoted by the large black point on the Y-axis). The lower dotted curve in Figure 11 shows the expected increase in σ_{meas} as a function of σ_{model}, and was calculated from the quadrature addition of the measurement LOD (33 pptv) with the σ_{model} value. The upper dotted curve gives a conservative upper limit to this function by assuming that the 1-minute LOD was as high as 50 pptv throughout TRACE-P. Although the LOD for some data points may be as high as 50 pptv, the majority of measurements exhibit LODs closer to 33 pptv [*Wert et al.*, 2003]. One should note that our calculation for the expected increase in both cases is only an approximation, since it assumes constant LOD and random and normally distributed measurement and model values in each leg. Nevertheless the above calculations capture reasonably well the bounds for the expected increase in σ_{meas} as a function of σ_{model}.

[42] For the 35 cloud-free intermediate horizontal flight legs (average measured CH_2O = 99 pptv) in Figure 11, the σ_{meas} averages 61% higher than the expected values from the lower dotted curve. One obtains nearly identical results employing CH_2O measurements uncorrected for the small methanol interference, indicating that the methanol correction does not play a role in the observed extra measurement variance. For the cloud-free fresh emission data (average measured CH_2O = 114 pptv), σ_{meas} averages 81% higher than the expected values from the lower dotted curve, while the corresponding data for in-cloud measurements (average CH_2O = 406 pptv), yields a σ_{meas} that is 68% higher than that modeled. Although the extra measurement variance relative to that modeled at the higher concentrations is

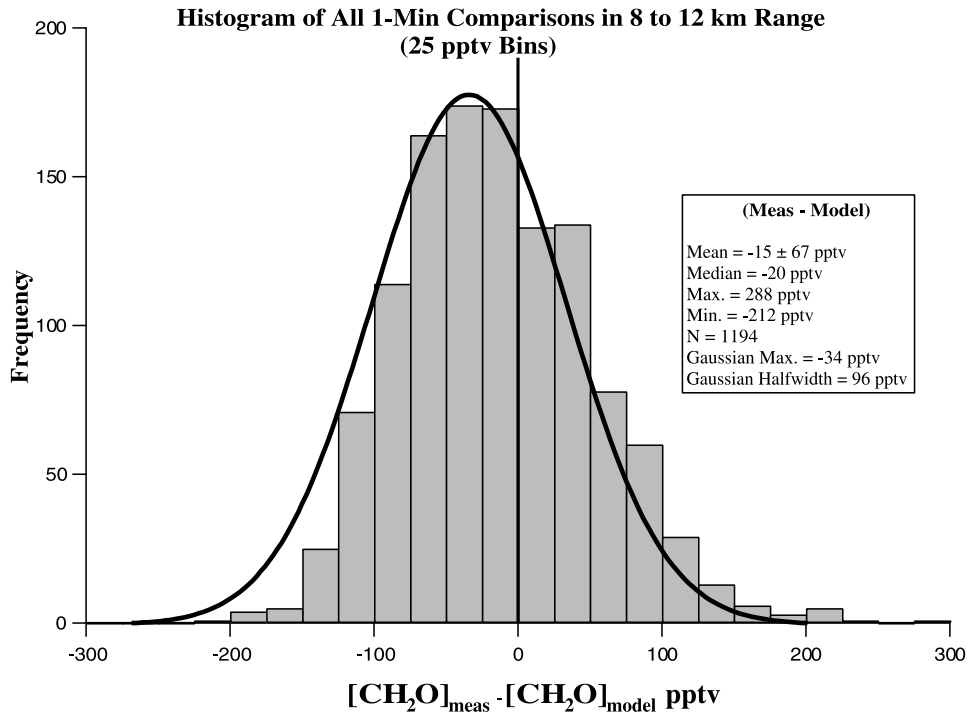

Figure 12. Histogram of time coincident 1-minute (measurement-model) differences for all longitudes combined for the 8–12 km altitude region during TRACE-P.

reasonable given the model limitations, the origin of the extra measurement variance for the lower concentration cloud-free intermediate legs is not readily apparent. However, the 12 more restrictive background legs (average CH_2O = 61 pptv) in all but a few cases fall very close to the expected lower curve based upon the quadrature addition of the measurement LOD with the σ_{model} value. In fact, the average ratio of observed to expected σ_{meas} in Figure 11 is 1.15, indicating little if any extra measurement variance for cloud-free background measurements.

[43] The above observations point to the important inference that even small to modest increases in the tracers of Tables 1a and 1b result in "lower model variance" relative to measurements. While the majority of points in Figure 11 have σ_{meas} and concentrations close to the measurement LOD, it is important to note that in 91% (N = 32) of the 35 cloud-free intermediate legs, σ_{meas} is higher than the lower expectation curve. Even if one conservatively uses the upper expectation curve, 66% (N = 23) of the 35 cloud-free intermediate legs show this reduced model variance. This implies that even after measurement-model systematic differences are eliminated, that unless one carefully eliminates all comparison points with small to modest elevations in the various tracers and precursors, one may very well expect to encounter box model results that underpredict the ambient variance. Clearly, additional studies to further investigate this finding are needed, particularly studies with improved measurement LODs.

6. Measurement-Model Comparisons at 8–12 km

[44] A number of studies have pointed to the potential importance of CH_2O as a source of HO_x in the upper troposphere from 8 to 12 km [e.g., *Crawford et al.*, 1999; *Jaeglé et al.*, 2000; *Heikes et al.*, 2001, and references therein], and the limited number of observations generally have revealed model underpredictions. For example, *Jaeglé et al.* [2000] report CH_2O model underpredictions by factors of 2–3 during the SONEX campaign, and point to the fact that model results fail to capture the observed variability. This study raises the possibility that additional sources of CH_2O, such as heterogeneous conversion of methanol on aerosols, may be important. Our TRACE-P CH_2O results give an additional opportunity to assess this possibility in the 8–12 km range.

[45] Figure 12 displays a histogram for all 1-minute (measurement-model) differences (N = 1194) in this altitude range for all longitudes. As can be seen by the mean (−15 pptv) and median (−20 pptv) differences, the overall agreement is quite good. It is not clear if the negative mean and medians are due to imperfect CH_2O scrubbing and/or over correction for the methanol interference. Based on lab tests and our NARE-97 studies, we believe that any scrubber breakthrough should be less than 10 to 20 pptv, and comparisons without applying the methanol correction yield mean and median (measurement-model) differences of 24 and 14 pptv, respectively. Therefore, it is quite possible that the overall differences may be close to 0 or slightly positive. In addition, the measurement and model distributions widths (10 to 90%) for horizontal leg averages in the 8–12 km range are nearly identical (measurement width = 78 pptv compared to 74 pptv for model width). Like the majority of our TOPSE comparisons up to 8 km, the above observations indicate that additional CH_2O sources and mechanisms, and hence additional sources of HO_x, which have been speculated in other studies, are not evident in the 8–12 km range during TRACE-P. However, it is important

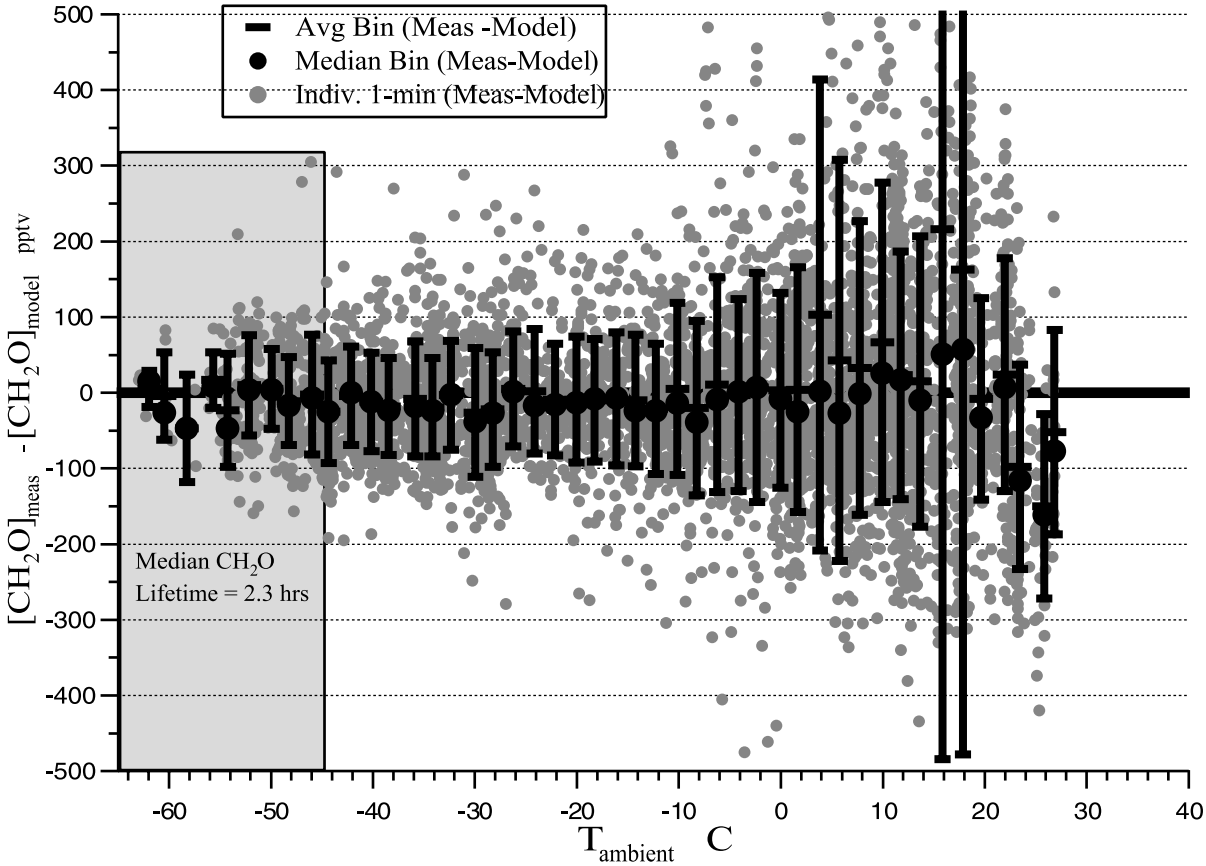

Figure 13. One-minute (measurement-model) as a function of ambient temperature in °C (gray points). The differences are also averaged into 2°C temperature bins, and the resulting bin average ±1σ and median are shown by the dark symbols.

to point out that such additional sources of CH_2O in the middle to upper troposphere cannot be ruled out in each and every case. Employing an earlier version of the TDLAS system discussed herein, Fried and colleagues observed CH_2O concentrations that were ~ a factor of 2 higher than those modeled [*Frost et al.*, 2002]. In addition, during certain situations during the TOPSE 2000 study significant model underpredictions were also observed, as will now be discussed.

7. (Measurement-Model) Temperature Dependence

[46] During the TOPSE 2000 study *Fried et al.* [2003] reported model CH_2O underpredictions by as much as 392 pptv (median underprediction of 132 pptv) in the 6–8 km altitude range for clean background conditions at high latitudes (latitudes > 57°N) under cold and dark conditions. At sampling temperatures starting at ~−45°C, *Fried et al.* [2003] observed an increase in the bin-averaged (measurement-model) discrepancy with decreasing temperature during the early deployments (February to April 2000) under dark conditions. Numerous possibilities for this discrepancy were investigated, but *Fried et al.* [2003] found no compelling evidence to support any of the hypotheses. TRACE-P provided another opportunity to study this effect but only at much higher light levels than TOPSE; at very low temperatures <−45 °C, the median TRACE-P CH_2O lifetime was ~2.3 hours compared to ~10 hours during TOPSE. In both field studies photolysis typically represents >94% of the total CH_2O destruction rate. Figure 13 displays the TRACE-P (measurement-model) comparison as a function of temperature for all the comparison points (median altitude = 10.7 km) as well as averages in 2°C temperature bins, the same format as that presented by *Fried et al.* [2003] during TOPSE. In contrast to TOPSE, the binned-average data of TRACE-P reveals no temperature dependence to the comparison, reinforcing the speculation by *Fried et al.* [2003] that low light levels may also be important in this regard. Under such conditions, long-range transport of CH_2O from lower latitudes can play a bigger role.

8. CH_2O Measurements in the Lower Marine Troposphere

[47] The LMT has been postulated to be both a source and sink for gas-phase CH_2O. For example, *Carlier et al.* [1986], *Zhou and Mopper* [1993, and references therein], and *Singh et al.* [2001], to name a few, suggest that oxygenated organics like CH_2O may be produced by the photochemical degradation of dissolved organic matter in the ocean surface. By contrast, numerous potential sinks for CH_2O in the LMT have also been reported. Such studies include the reaction of CH_2O with free radicals [*Carlier et*

Table 2. Seven Lower Marine Tropospheric Horizontal Flight Legs Where Marine Aerosol Haze (Cloud Index 1) was Encountered Without Fresh Pollution[a]

Longitude Bin	Flight	Leg Time Start	Leg Time Stop	Palt, km	N	Meas. – Model, pptv	Change, %
EP	4	20:34	21:04	<0.5	28	4	9
CP	5	22:45	22:54	1.1	9	−255	−73
CP	5	00:24	00:35	1.4	8	−177	−57
CP	5	02:46	03:20	<0.5	31	−184	−58
WP	11	04:11	04:35	<0.5	20	−152	−49
WP	11	05:50	06:02	<0.5	10	−20	−10
CP	18	04:42	05:12	<0.5	17	32	9

[a]The measurements were averaged over the leg and the (measurement-model) differences were calculated from the average point-by-point differences in each leg, and N gives the number of such comparisons. All times are UTC. The % change for each leg was calculated from (measurement-model)/model × 100.

al., 1986]; scavenging by water droplets and aerosols [*Thompson*, 1980; *Klippel and Warneck*, 1978]; uptake in clouds [*Barth et al.*, 2003]; dry deposition to the ocean surface [*Thompson*, 1980]; the laboratory experiments of *Zhou and Mopper* [1990], which indicated a very large undersaturation of CH_2O in seawater, and hence the expectation that the oceans are a net sink of CH_2O. *Wagner et al.* [2002] also raise the possibility that in high biogenic areas of the oceans, the surface seawater may revert from a net sink of CH_2O to a net source. The *Wagner et al.* [2002] study also discusses the possibility that free tropospheric air with its lower CH_2O concentration becomes entrained in the LMT, thus lowering ambient concentrations significantly below steady state.

[48] The measurement-model comparisons of the present study in the LMT allow us to examine this region. The LMT comparisons in the CP longitude bin of Figure 5 suggest that CH_2O sink processes are operative. This assessment, however, is complicated by a number of factors including: pollution, clouds which are often observed in the LMT, potential heterogeneous chemistry on marine aerosols, potential uptake of CH_2O precursors in clouds and in the ocean, and potential entrainment of free tropospheric air. As in previous sections, fresh pollution was easily identified and excluded from this analysis by examining various NMHC precursors and tracers, and 12 LMT legs were identified that were either very clean or only slightly elevated. Of the 12 legs, five legs were excluded because CH_3OOH measurements were not available and the calculated model values that were employed were significantly elevated relative to measurements carried out close in time. Of the remaining seven legs, all were primarily characterized by LMT haze (cloud index 1) where the liquid water content was <0.02 g m^{-3} and more typically <10^{-3}. These seven legs and the associated conditions are listed in Table 2. As can be seen, CH_2O uptake was observed in five of the seven legs, and in four cases the uptake averaged 59%.

[49] Figure 14 (9 points in the shaded rectangle) displays CH_2O uptake in one of the LMT flight legs. This leg occurred on flight 5 (second leg in Table 2 at 18°N latitude, 185° longitude) in the CP longitude bin west of Hawaii.

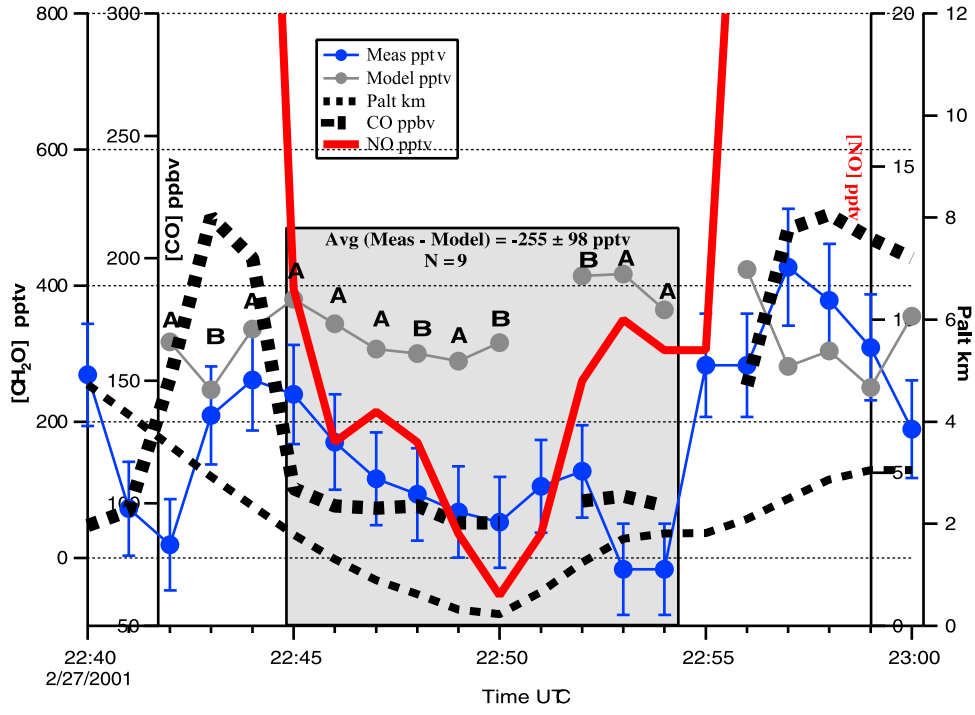

Figure 14. One of seven relatively clean lower marine tropospheric legs. This leg was acquired during flight 5 just west of Hawaii in the CP region. The 1-minute CH_2O measurements are given in blue along with the total measurement uncertainty (2σ level) while the modeled values are shown by the gray points. The profiles of CO (dark dotted points) and NO (solid red line) are also given. Points labeled by "A" employed measured CH_3OOH in the model calculations of CH_2O, while those labeled by "B" employed the modeled CH_3OOH in these calculations.

Here the NO concentrations averaged 6 pptv and the measurements of CH_3OOH (average = 901 pptv) were available (points "A") in six of the nine comparisons. The calculated CH_3OOH (average = 931 pptv) for the other 3 points (points "B") is close to the measurements, and as a result the calculated CH_2O does not depend upon which CH_3OOH is used in the model. Thus the inconsistency evident in Figure 1 is not present here and the measurement-model CH_2O comparison can be used to assess LMT uptake of CH_2O. The potential temperature profile (not shown) indicates an inversion located at 1.8 km, but exhibits a moist adiabatic lapse rate below. The inversion coincides with a jump in CO, NO, and CH_2O in Figure 14, however, the layer below shows strong, continuous vertical gradients too. This is observed for potential temperature and water vapor as well, and it indicates that the layer sampled is not a traditional, well-mixed MBL, and hence we refer to this buffer layer as the LMT. Not until the airplane reaches below 300 m do the profiles show initial traces of being well mixed. The layer below the strong inversion at 1.8 km is indeed different, however, in that it is characterized by considerable marine aerosol haze.

[50] The agreement in the measured and modeled CH_2O on both sides of the LMT horizontal leg of Figure 14, while not perfect, is reasonable. The (measurement-model) difference for the 2 points on both sides of the LMT run averages -27 ± 123 pptv. This is contrasted by the LMT run where the measurements (error bars denote the total 2σ uncertainties) drop precipitously from 240 pptv (22:45) to 52 pptv (22:50) while the modeled CH_2O only changes from 380 pptv to 316 pptv. The (measurement-model) difference for the 9 points in the LMT averages -255 ± 98 pptv, which when compared to an average model value of 348 pptv yields a 73% uptake. Because most of the chemical species and thermodynamic variables indicate fairly strong stratification, we assume that efficient turbulent mixing to the ocean surface is not occurring and thus we conclude that oceanic uptake cannot explain the observed disagreement between the model and the measurements in this case. Likewise, entrainment of cleaner free tropospheric air down into the LMT layer being sampled can also be ruled out since the strong inversion at 1.8 km reduces such downward mixing, and to the extent that it does occur in this case, it would transport air with elevated CH_2O levels instead of cleaner background air downward.

[51] The dry surface area density (aerosol diameters between 0.1 to 0.75 μm) ranged between $\sim$5 to $\sim$15 $\mu m^2\ cm^{-3}$ over the time period from 22:45 to 22:50 and averaged 5 $\mu m^2\ cm^{-3}$. Assuming an irreversible heterogeneous loss of formaldehyde that is not gas phase diffusion limited employing a reaction probability (γ) of 0.02 [*Jayne et al.*, 1996] and the maximum surface area density of 15 $\mu m^2\ cm^{-3}$, one calculates a heterogeneous loss rate of $\sim 3 \times 10^{-5}\ s^{-1}$, which is $\sim$7% of that required to reconcile the model overestimation. This calculation, however, is highly uncertain because the γ from *Jayne et al.* [1996] is for 70 weight % H_2SO_4 aerosols, whereas the aerosol composition for the present measurements is unknown. In addition, our aerosol surface area density is also highly uncertain due to the drying process upon sampling, and under the present relative humidity conditions (90%) it is possible that surface area density may be as much as a factor of 4 larger [*Swietlicki et al.*, 2000], resulting in a loss rate that is $\sim$28% of that required. Therefore, although heterogeneous uptake of CH_2O on LMT aerosols does not appear to reconcile the model overestimations, it cannot be ruled out, at least as a partial contributor. What is very interesting is that the measurements and model overestimations of the present study are very similar to those reported by *Jacob et al.* [1996] in the South Atlantic near the ocean surface. In that study, *Jacob et al.* [1996] report measured CH_2O concentrations of 0.11 ppbv compared to modeled values of 0.41 ppbv, and raise the possibility of a large unknown CH_2O sink near the ocean surface.

[52] Table 2 shows three additional LMT legs with very large CH_2O uptake, possibly on marine aerosol haze. The very large CH_2O depletion from whatever cause is a fairly important new observation that warrants further study. Uptake on marine aerosols has been speculated by *Zhou et al.* [1996], but *Wagner et al.* [2002] dismiss its importance based on the MOCCA model, which considers standard gas-phase chemistry, the effect of aerosols as well as halogen chemistry. *Wagner et al.* [2002] conclude that given our current understanding of liquid phase chemistry of CH_2O, the direct effect of aerosols on the CH_2O budget is not significant in the remote MBL.

[53] Unfortunately, we have no knowledge of the recent past history of the four LMT flight legs in Table 2 showing large CH_2O uptake in relation to cloud exposure (i.e., whether or not ambient CH_2O was exposed to marine clouds in the near past prior to our measurements). Hence one cannot rule out that our observations of LMT uptake may reflect uptake in marine clouds in the near past prior to our measurements.

9. Summary and Conclusions

[54] The present paper describes an extensive set of 1-minute airborne CH_2O measurements acquired by tunable diode laser absorption spectroscopy during the TRACE-P study and comprehensive comparisons with a steady state box model. Measurements were segregated into three longitude bins and eight altitude bins, with the western Pacific (WP) bin revealing the highest CH_2O concentrations, as expected based upon a median CH_2O lifetime of 2.2 hours and the close proximity to large Asian sources. All three-longitude altitude profiles revealed a fall off in CH_2O with altitude.

[55] Measurement-model comparisons were carried out using a number of different approaches. Above $\sim$2.5 km, where the influences of large anthropogenic pollution from Asian outflow and marine boundary layer (MBL) aerosol uptake were minimized, measurements and model medians binned according to altitude were in excellent agreement to within $\pm$37 pptv. Likewise, we obtained a near unity slope (0.98 ± 0.03) from a bivariate fit of the measurements, averaged into 25 pptv model bins, versus the modeled concentrations for values up to $\sim$450 pptv. Similar to our overall TOPSE results, the present study indicates no systematic bias on average between CH_2O measurements and box model results out to model values $\sim$450 pptv. However, as in TOPSE, the model results progressively underpredict the observations at higher concentrations due to a breakdown in the box model steady state assumption.

[56] Despite the overall agreement below 450 pptv, we observed larger than expected scatter in individual point-to-point comparisons, and the effects of clouds and LMT aerosols were shown to be important in this regard. The measurement-model variance was further studied employing horizontal flight legs to eliminate complicating factors. With the exception of 12 cloud-free background legs, all horizontal flight legs revealed measurement variance ~60 to 80% higher than that modeled. This points to the important inference that even after measurement-model systematic differences are eliminated, that unless one carefully eliminates all comparison points with small to modest elevations in the various tracers and precursors, one may very well expect to encounter box model results that underpredict the ambient variance.

[57] A number of measurement-model comparisons for CH_2O were also carried out for a variety of specific conditions, including measurements in the upper troposphere (8–12 km), measurements in clouds, and measurements in the LMT. In the upper troposphere, the overall mean and median (measurement-model) difference was -15 ± 67 pptv, and -20 pptv, respectively. Contrary to a number of previous studies, the present study suggests that additional sources of CH_2O at midlatitudes over the Pacific in the upper troposphere were not necessary to explain the present observations. However, this does not rule out the possibility that additional CH_2O sources, such as unmeasured oxygenated volatile organic carbon compounds postulated by *Frost et al.* [2002], may be important in some cases in the middle to upper troposphere. In addition, unlike TOPSE, no divergence in the measurement-model agreement was observed as a function of temperature, reinforcing the speculation by *Fried et al.* [2003] that low light levels may also be important in reconciling CH_2O observations at high latitudes in the upper troposphere.

[58] A number of events were identified in the present study where CH_2O uptake in clouds has been observed where the liquid water content was typically >0.02 g m^{-3}. An overall comparison of median (measurement-model) differences for in-cloud versus cloud-free data revealed that the box model persistently overpredicted the observations, in one case by as much as 24% relative to cloud-free data. However, uptake of CH_2O in clouds is complicated by pollution. In fact, an average in-cloud uptake of CH_2O of 56% has been observed on one occasion (peak uptake of 85%) where fresh pollution was not evident. Corresponding measurements in the LMT where haze was observed also revealed large CH_2O uptake. Over the seven flight legs where fresh pollution was not evident, the CH_2O loss averaged 33% and attained a loss rate as high as 73% during one particular leg. However, one cannot rule out the possibility that marine clouds prior to our measurements may be playing a large role instead of aerosol haze. Regardless, these are important new observations and further studies are needed to fully understand all the processes that affect ambient CH_2O concentrations.

[59] **Acknowledgments.** The National Center for Atmospheric Research is operated by the University Corporation for Atmospheric Research under the sponsorship of the National Science Foundation. This research was supported by funds from the National Aeronautics and Space Administration's Global Tropospheric Experiment. The authors wish to thank the dedicated staff of the ACD machine and electronics shops for their assistance, and the NASA DC-8 staff and crew for all their valuable support both before and during the field mission.

References

Ayers, P. G., R. W. Gillett, H. Granek, C. de Serves, and R. A. Cox, Formaldehyde production in clean marine air, *Geophys. Res. Lett.*, *24*, 401–404, 1997.

Barth, M. C., S. Sillman, R. Hudman, M. Z. Jacobson, C.-H. Kim, A. Monod, and J. Liang, Summary of the cloud chemistry modeling intercomparison: Photochemical box model simulation, *J. Geophys. Res.*, *108*(D7), 4214, doi:10.1029/2002JD002673, 2003.

Calvert, J. G., R. Atkinson, J. A. Kerr, S. Madronich, G. K. Moortgat, T. J. Wallington, and G. Yarwood, *The Mechanisms of Atmospheric Oxidation of the Alkenes*, pp. 371–379, Oxford Univ. Press, New York, 2000.

Carlier, P., H. Hannachi, and G. Mouvier, The chemistry of carbonyl compounds in the atmosphere: A review, *Atmos. Environ.*, *20*, 2079–2099, 1986.

Crawford, J. H., et al., Assessment of upper tropospheric HO_x sources over the tropical Pacific based on NASA GTE/PEM data: Net effect on HO_x and other photochemical parameters, *J. Geophys. Res.*, *104*, 16,255–16,273, 1999.

de Serves, C., Gas phase formaldehyde and peroxide measurements in the Arctic atmosphere, *J. Geophys. Res.*, *99*, 25,391–25,398, 1994.

Eisele, F. L., et al., Summary of measurement intercomparisons during TRACE-P, *J. Geophys. Res.*, *108*(D20), 8791, doi:10.1029/2002JD003167, in press, 2003.

Fried, A., S. Sewell, B. Henry, B. P. Wert, T. Gilpin, and J. R. Drummond, Tunable diode laser absorption spectrometer for ground-based measurements of formaldehyde, *J. Geophys. Res.*, *102*, 6253–6266, 1997a.

Fried, A., et al., Photochemistry of formaldehyde during the 1993 tropospheric OH photochemistry experiment, *J. Geophys. Res.*, *102*, 6283–6296, 1997b.

Fried, A., B. Henry, B. Wert, S. Sewell, and J. R. Drummond, Laboratory, ground-based, and airborne tunable diode laser systems: Performance characteristics and applications in atmospheric studies, *Appl. Phys. B*, *67*, 317–330, 1998.

Fried, A., Y.-N. Lee, G. Frost, B. Wert, B. Henry, J. R. Drummond, G. Hubler, and T. Jobson, Airborne CH_2O measurements over the North Atlantic during the 1997 NARE campaign: Instrument comparisons and distributions, *J. Geophys. Res.*, *107*(D4), 4039, doi:10.1029/2000JD000260, 2002.

Fried, A., et al., Tunable diode laser measurements of formaldehyde during the TOPSE 2000 Study: Distributions, trends, and model comparisons, *J. Geophys. Res.*, *108*(D4), 8365, doi:10.1029/2002JD002208, 2003.

Frost, G. J., et al., Comparison of box model calculations and measurements of formaldehyde from the 1997 North Atlantic Regional Experiment, *J. Geophys. Res.*, *107*(D8), 4060, doi:10.1029/2001JD000896, 2002.

Gilpin, T., et al., Intercomparison of six ambient [CH_2O] measurement techniques, *J. Geophys. Res.*, *102*, 21,161–21,188, 1997.

Heikes, B., et al., Formaldehyde methods comparison in the remote lower troposphere during the Mauna Loa Photochemistry Experiment 2, *J. Geophys. Res.*, *101*, 14,741–14,755, 1996.

Heikes, B., J. Snow, P. Egli, D. O'Sullivan, J. Crawford, J. Olson, G. Chen, D. Davis, N. Blake, and D. Blake, Formaldehyde over the central Pacific during PEM-Tropics B, *J. Geophys. Res.*, *106*, 32,717–32,731, 2001.

Jacob, D. J., et al., Origin of ozone and NO_x in the tropical troposphere: A photochemical analysis of aircraft observations over the South Atlantic basin, *J. Geophys. Res.*, *101*, 24,235–24,250, 1996.

Jaeglé, L., et al., Photochemistry of HO_x in the upper troposphere at northern midlatitudes, *J. Geophys. Res.*, *105*, 3877–3892, 2000.

Jayne, J. T., D. R. Worsnop, C. E. Kolb, E. Swartz, and P. Davidovits, Uptake of gas-phase formaldehyde by aqueous acid surfaces, *J. Phys. Chem.*, *100*, 8015–8022, 1996.

Klippel, W., and P. Warneck, Formaldehyde in rain water and on the atmospheric aerosol, *Geophys. Res. Lett.*, *5*, 177–179, 1978.

Lee, M., B. G. Heikes, D. J. Jacob, G. Sachse, and B. Anderson, Hydrogen peroxide, organic hydroperoxide, and formaldehyde as primary pollutants from biomass burning, *J. Geophys. Res.*, *102*, 1301–1309, 1997.

Liu, S. C., et al., A study of the photochemistry and ozone budget during the Mauna Loa Observatory experiment, *J. Geophys. Res.*, *97*, 10,463–10,471, 1992.

Lowe, D. C., and U. Schmidt, Formaldehyde (HCHO) measurements in the nonurban atmosphere, *J. Geophys. Res.*, *88*, 10,844–10,858, 1983.

Neri, F., G. Saitta, and S. Chiofalo, An accurate and straightforward approach to line regression analysis of error-affected experimental data, *J. Phys. E Sci. Instrum.*, *22*, 215–217, 1989.

Olson, J. R., et al., Seasonal differences in the photochemistry of the South Pacific: A comparison of observations and model results from PEM-Tropics A and B, *J. Geophys. Res.*, *106*, 32,749–32,766, 2001.

Russell, L. M., D. H. Lenschow, K. K. Laursen, P. B. Krummel, S. T. Siems, A. R. Bandy, D. C. Thornton, and T. S. Bates, Bidirectional mixing in an ACE 1 marine boundary layer overlain by a second turbulent layer, *J. Geophys. Res.*, *103*, 16,411–16,432, 1998.

Sigsby, J. E., S. Tejada, W. Ray, J. M. Lang, and J. W. Duncan, Volatile organic compound emissions from 46 in-use passenger cars, *Environ. Sci. Technol.*, *21*, 466–475, 1987.

Singh, H., Y. Chen, A. Staudt, D. Jacob, D. Blake, B. Heikes, and J. Snow, Evidence from the Pacific troposphere for large global sources of oxygenated organic compounds, *Nature*, *410*, 1078–1081, 2001.

Swietlicki, E., et al., Hygroscopic properties of aerosol particles in the northeastern Atlantic during ACE-2, *Tellus, Ser. B*, 201–227, 2000.

Thompson, A. M., Wet and dry removal of tropospheric formaldehyde at a coastal site, *Tellus*, *32*, 376–383, 1980.

Tyndall, G. S., R. A. Cox, C. Granier, R. Lesclaux, G. K. Moortgat, M. J. Pilling, A. R. Ravishankara, and T. J. Wallington, Atmospheric chemistry of small organic peroxyl radicals, *J. Geophys. Res.*, *106*, 12,157–12,182, 2001.

Wagner, V., R. von Glasow, H. Fischer, and P. J. Crutzen, Are CH_2O Measurements in the Marine boundary layer suitable for testing the current understanding of CH_4 photooxidation?: A model study, *J. Geophys. Res.*, *107*(D3), 4029, doi:10.1029/2001JD000722, 2002.

Weller, R. O., O. Schrems, A. Boddenberg, S. Gäb, and M. Gautrois, Meridional distribution of hydroperoxides and formaldehyde in the marine boundary layer of the Atlantic (48°N–35°S) measured during the Albatross campaign, *J. Geophys. Res.*, *105*, 14,401–14,412, 2000.

Wennberg, P. O., et al., Hydrogen radicals, nitrogen radicals, and the production of O_3 in the upper troposphere, *Science*, *279*, 49–53, 1998.

Wert, B. P., A. Fried, B. Henry, and S. Cartier, Evaluation of inlets used for the airborne measurement of formaldehyde, *J. Geophys. Res.*, *107*(D13), 4163, doi:10.1029/2001JD001072, 2002.

Wert, B. P., A. Fried, S. Rauenbuehler, J. Walega, and B. Henry, Design and performance of a tunable diode laser absorption spectrometer for airborne formaldehyde measurements, *J. Geophys. Res.*, *108*(D12), 4350, doi:10.1029/2002JD002872, 2003.

Zhou, X., and K. Mopper, Apparent Partition Coefficients of 15 Carbonyl Compounds between air and seawater and between air and freshwater: Implications for air-sea exchange, *Environ. Sci. Technol.*, *24*, 1864–1869, 1990.

Zhou, X., and K. Mopper, Carbonyl compounds in the lower marine troposphere over the Caribbean Sea and Bahamas, *J. Geophys. Res.*, *98*, 2385–2392, 1993.

Zhou, X., Y.-N. Lee, L. Newman, X. Chen, and K. Mopper, Tropospheric formaldehyde concentration at the Mauna Loa Observatory during the Mauna Loa Observatory Photochemistry Experiment 2, *J. Geophys. Res.*, *101*, 14,711–14,719, 1996.

B. Anderson, J. Crawford, C. Jordan, J. Olson, and G. Sachse, Atmospheric Sciences Division, Langley Research Center, NASA, Mail Stop 483, Hampton, VA 23681, USA.

D. Blake, N. Blake, and S. Meinardi, Department of Chemistry, University of California, Irvine, Irvine, CA 92697-2025, USA.

G. R. Carmichael, Department of Chemical and Biochemical Engineering, University of Iowa, Iowa City, IA 52242-1000, USA.

I. Faloona, A. Fried, B. Lefer, R. Shetter, J. Walega, and B. Wert, Atmospheric Technology and Atmospheric Chemistry Divisions, National Center for Atmospheric Research, Boulder, CO 80301, USA. (fried@ucar.edu)

H. E. Fuelberg and C. M. Kiley, Department of Meteorology, Florida State University, Tallahassee, FL 32306-4520, USA.

C. Harward, SAIC, Langley Research Center, NASA, Mail Stop 472, Hampton, VA 23681-2199, USA.

B. Heikes and J. Snow, Graduate School of Oceanography/Center for Atmospheric Chemistry, University of Rhode Island, South Ferry Road, Narragansett, RI 02882-1197, USA.

D. O'Sullivan, Department of Chemistry, U.S. Naval Academy, Annapolis, MD 21401, USA.

W. Potter, Department of Chemistry and Biochemistry, University of Tulsa, Tulsa, OK 74104, USA.

S. T. Sandholm and D. Tan, School of Earth and Atmospheric Sciences, Georgia Institute of Technology, Atlanta, GA 30332, USA.

H. Singh, NASA Ames Research Center, Mail Stop 245-5, Moffett Field, CA 94035, USA.